Differences in mitochondrial activity trigger cell competition during early mouse development

Ana Lima[1,2,#] Gabriele Lubatti[3,4,5,#], Jörg Burgstaller[6], Di Hu[7], Alistair Green[8], Aida Di Gregorio[1], Tamzin Zawadzki[1], Barbara Pernaute[1,9], Elmir Mahammadov[3,4,5], Marian Dore[2], Juan Miguel Sanchez[1], Sarah Bowling[1], Margarida Sancho[1], Mohammad Karimi[2], David Carling[2], Nick Jones[8], Shankar Srinivas[7], Antonio Scialdone[3,4,5*] and Tristan A. Rodriguez[1,*]

[1] National Heart and Lung Institute, Imperial College London, UK

[2] MRC London Institute of Medical Sciences (LMS), Institute of Clinical Sciences, Imperial College London, UK

[3] Institute of Epigenetics and Stem Cells, Helmholtz Zentrum München, Munich, Germany

[4] Institute of Functional Epigenetics, Helmholtz Zentrum München, Neuherberg, Germany

[5] Institute of Computational Biology, Helmholtz Zentrum München, Neuherberg, Germany

[6] Institute of Animal Breeding and Genetics, University of Veterinary Medicine, Vienna, Austria

[7] Department of Physiology, Anatomy and Genetics, University of Oxford, Oxford, UK

[8] Department of Mathematics, Imperial College London, UK.

[9] Current address: Centre for Genomic Regulation (CRG), The Barcelona Institute of Science and Technology, Dr. Aiguader 88, Barcelona 08003, Spain

[#] Both these authors contributed equally

* Authors for correspondence: antonio.scialdone@helmholtz-muenchen.de; tristan.rodriguez@imperial.ac.uk

Summary

Cell competition is emerging as a quality control mechanism that eliminates unfit cells in a wide range of settings from development to the adult. However, the nature of the cells normally eliminated by cell competition and what triggers their elimination remains poorly understood. Here we have performed single cell transcriptional profiling of early mouse embryos and find that the cells eliminated show the hallmarks of cell competition, are mis-patterned and have mitochondrial defects. We demonstrate that mitochondrial defects are common to a range of different loser cell types and that manipulating mitochondrial function is sufficient to trigger competition. Importantly, we show that in the embryo loser epiblast cells display mitochondrial DNA mutations and that even small changes in mitochondrial DNA sequence can influence the competitive ability of the cell. Our results therefore suggest that cell competition is a purifying selection that optimises metabolic output prior to gastrulation.

Running title: Cell competition and mitochondrial selection

Keywords: mitochondria, mtDNA, mouse development, cell competition, purifying selection

Introduction

During the early stages of mammalian development, the cellular and molecular landscape is profoundly remodelled. As embryonic cells approach gastrulation, when the precursors of all embryonic tissues are specified, they need to rewire the transcriptional, epigenetic, metabolic and signalling networks that govern cell identity (Kojima et al., 2014). These changes are accompanied by a marked acceleration in the proliferation rate (Snow, 1977) and need to be orchestrated with the different morphogenetic processes that re-shape the embryo (reviewed in (Stower and Srinivas, 2018). The scale of this remodelling creates the potential for the emergence of abnormal cells that need to be removed to prevent them from contributing to the soma or germline during development. This requirement implies that there must be stringent cell fitness quality control mechanisms acting around the time of gastrulation. One such control has been postulated to be cell competition, a fitness sensing mechanism eliminating cells that, although viable, are less fit than their neighbours (reviewed in (Bowling et al., 2019; Diaz-Diaz and Torres, 2019; Madan et al., 2018). During cell competition, the cells that are eliminated are generically termed losers, while the fitter cells that survive are referred to as winners.

Cell competition has been primarily studied in *Drosophila*, where it was first described in the imaginal wing disc (Morata and Ripoll, 1975). Since then, it has also been found to be conserved in mammals. For example, in the mouse embryo between E5.5 and E6.5 cell competition has been proposed to eliminate less-fit cells from the epiblast, the pluripotent tissue that generates the three primary germ-layers (Claveria et al., 2013; Sancho et al., 2013). Importantly, in the time-window when cell competition acts, about one third of epiblast cells are eliminated by apoptosis (Bowling et al., 2018). These cells are marked by a loss of mTOR signalling, a read-out of loser status during cell competition *in vitro* (Bowling et al., 2018). This suggests that cell competition is the primary cause of this cell elimination. Other markers of those cells eliminated in the early post-implantation embryo have been identified as relative low c-MYC expression, high P53 expression or elevated levels of ERK phosphorylation (Bowling et al., 2018; Claveria et al., 2013; Diaz-Diaz et al., 2017; Sancho et al., 2013), that together could be considered as a cell competition signature.

In spite of the advance that identifying these markers signifies, we still do not know what overarching cellular and molecular features define the cells eliminated by cell competition in mouse. Using embryonic stem cells (ESCs) and embryo chimeras we have shown that mis-patterned cells, autophagy deficient cells and karyotypically abnormal cells are all eliminated upon differentiation by cell competition (Bowling et al., 2018; Sancho et al., 2013). Cell competition has also been shown to eliminate pluripotent cells that differentiate precociously (Diaz-Diaz et al., 2017) or that are not properly specified (Hashimoto and Sasaki, 2019). Therefore, a variety of different defective cell types can be eliminated by cell competition, but which is the underlying cause for their elimination remains poorly understood.

Mitochondria, with their diverse cellular functions ranging from determining the bioenergetic output of the cell to regulating its apoptotic response, are strong candidates for determining competitive cell fitness. During early mouse development mitochondria undergo profound changes in their shape and activity (reviewed in (Lima et al., 2018). In the pre-implantation embryo mitochondria are rounded, fragmented and contain sparse cristae, but upon implantation they fuse to form complex networks with mature cristae (Zhou et al., 2012). The mode of replication of the mitochondrial genome (mtDNA), that encodes for vital components of the bioenergetic machinery, also changes during early mouse development. After fertilization, mtDNA replication ceases and its copy number per cell decreases with every division until post-implantation stages, when mtDNA replication resumes (reviewed in (Lima et al., 2018). However, as the mutation rate of mtDNA is significantly higher than that of nuclear DNA (Allio et al., 2017; Khrapko et al., 1997) this increased replication most likely leads to an increased mutation load. A number of mechanisms have been proposed to reduce this mutation load, such as the bottleneck effect, purifying selection or biased segregation of mtDNA haplotypes (Burgstaller et al., 2014; Johnston et al., 2015; Latorre-Pellicer et al., 2019; Lee et al., 2012; Sharpley et al., 2012; Zhang et al., 2018). However, despite these mechanisms, inheritable mtDNA based diseases are reported with a prevalence of 5-15 cases per 100,000 individuals (Burgstaller et al., 2015; Gorman et al., 2016), highlighting both the importance and limitations of these selection mechanisms.

To understand the nature of the cells eliminated during early mouse post-implantation development we have analysed their transcriptional profile by single-cell RNA sequencing. Importantly, we have found that these cells share a cell competition signature. Analysis of the pathways mis-regulated in the cells eliminated identified mitochondrial dysfunction as a common feature. Furthermore, we demonstrate that manipulating mitochondrial activity either by disrupting mitochondrial dynamics or by introducing small mtDNA changes is sufficient to trigger cell competition during early mouse development. These results therefore pinpoint mitochondrial performance as a key cellular feature that determines the competitive ability of embryonic cells.

Results

Cells eliminated in the early mouse embryo have a distinct transcriptional profile

We have previously shown that in the early post-implantation mouse embryo about 35% of epiblast cells are eliminated and that these cells are marked by low mTOR signalling (Bowling et al., 2018). However, we currently do not understand the characteristics of these cells or what triggers their elimination. To answer these questions, we have analysed their transcriptional profile by single cell RNA sequencing (scRNA-seq). To ensure we can capture the eliminated cells, as we have done before (Bowling et al., 2018), we isolated embryos at E5.5 and cultured them for 16 hours in the presence of a caspase inhibitors (CI) or vehicle (DMSO) (Figure 1A and Figure S1A).

Unsupervised clustering of the scRNA-seq data revealed five clusters: two corresponding to extra-embryonic tissues (visceral endoderm and extra-embryonic ectoderm) and three that expressed epiblast marker genes (Figure 1B-C and Figure S1B-D). Interestingly, cells from CI- and DMSO-treated embryos are unequally distributed across the three epiblast clusters. In particular, one of these clusters (cluster 4) is only composed of cells from CI-treated embryos (Figure 1D-E). To establish the relationship between these epiblast clusters we computed a diffusion map (Angerer et al., 2016). For this, we selected only cells captured from CI-treated embryos, to eliminate possible confounding effects due to the caspase inhibitor (Figure 2A). However, when all epiblast cells are considered, the results remain unchanged (Figure S2A-C). This analysis identified a trajectory between the three epiblast clusters, with those cells unique to CI-treated embryos falling at one extreme end of the trajectory (corresponding to cluster 4; Figure 2A) and with those cells present in both DMSO and CI-treated embryos at the other (corresponding to cluster 1; Figure 2A and Figure S2A-C).

To further define the identity of the epiblast cells of CI-treated embryos we analysed the genes differentially expressed along the trajectory (see Methods and Figure S2D) using Ingenuity Pathway Analysis (IPA) to characterize gene signatures (Kramer et al., 2014). Importantly, we found that these differentially expressed genes fell under molecular and cellular function categories associated with cell death and survival, protein synthesis and nucleic acids (Figure 2B). Analysis of the factors with enriched targets within the genes differentially expressed along the trajectory revealed RICTOR (an mTOR component), TLE3, MYC, MYCN, P53 and IGFR (that is upstream of mTOR) as the top upstream regulators (Figure 2C). Breaking down the differentially expressed genes into those down-regulated or up-regulated along the winner-to loser trajectory revealed that the targets of RICTOR, MYC, MYCN and IGFR primarily fell within the down-regulated genes (Supplementary Tables 1 and 2). P53 activated targets were preferentially up-regulated and P53 repressed targets were preferentially down-regulated (Figure S2E-F). Moreover, genes related to protein synthesis were primarily found to be downregulated.

The first identified trigger of cell competition were differences in protein synthesis (Morata and Ripoll, 1975), therefore the observation that the genes differentially expressed along the trajectory fall into cell death and protein synthesis categories, as well as being mTOR, MYC and P53 targets strongly suggests that cells at each end of the trajectory are the winners and losers of cell competition. For this reason, we hereafter refer to those epiblast cells unique to CI-treated embryos as “loser” epiblast cells and to those at the opposite end of the trajectory as the “winner” epiblast cells. Those cells lying between these two populations on the trajectory are considered “intermediate”. Using this knowledge we can define a diffusion pseudotime (dpt) coordinate (Haghverdi et al., 2016) originating in the “winner” cluster that tracks the position of cells along the

108 trajectory and that can be interpreted as a “losing score”, i.e., it quantifies how strong the signature
109 of the “losing” state is in the transcriptome of a cell (see Figure 2D-E).

110 Loser cells show a signature of mis-patterning

111 The most notable change that embryonic cells undergo during early development is the onset of
112 differentiation. During this process cells transit from naïve to primed pluripotency and then undergo
113 germ layer specification (Nichols and Smith, 2009). For this reason, we analysed the expression
114 of pluripotency and differentiation markers as a function of the losing score of epiblast cells (Figure
115 2F). We found that loser cells (with high losing scores) have lower levels of expression of genes
116 such as *Fgf5* and *Tdgf1*, which are characteristic of the primed pluripotency state. In contrast to
117 this, they displayed high levels of expression of some naïve pluripotency markers such as *Klf4*
118 and *Klf5*, but not of others, such as *Rex1* (*Zfp42*). Analysis of lineage specific markers revealed a
119 complex pattern. For example, some loser cells showed high expression of the endoderm marker
120 *Sox17*, but not of *Gata6*. Something similar was observed for neuroectoderm markers, whereby
121 loser cells showed significantly higher expression of *Neurod1* than winner cells, but comparable
122 levels of *Sox1*.

123 Plotting the levels of markers of naïve pluripotency and germ layers against each other for single
124 cells revealed that some loser epiblast cells expressed higher levels of both naïve pluripotency
125 and germ-layer markers than normal epiblast cells (Figure 2G). Together, these data suggest that
126 loser epiblast cells represent a generic mis-patterned state, rather than precocious or delayed
127 differentiation.

128 Loser cells are characterised by defects in mitochondrial function

129 We next analysed using IPA the cellular pathways mis-regulated in loser epiblast cells and found
130 that the top two pathways (mitochondrial dysfunction and oxidative phosphorylation) are related
131 to mitochondrial function (Figure 3A). Detailed inspection of the oxidative phosphorylation
132 signature in loser versus normal epiblast cells indicated that 92.6% of the genes in this pathway
133 were mis-regulated (Figure 3A), including the majority of genes encoding proteins of the five
134 complexes (Complexes I to V) of the electron transport chain (ETC)(Figure 3B), that were down-
135 regulated along the winner-to-loser trajectory (Supplementary Table 1). For example, we found a
136 down-regulation along the winner to loser trajectory of the mitochondrial DNA encoded *mt-Nd3*
137 and *mt-Atp6* (Figure 3C), of regulators of mitochondrial dynamics such as *Opa1,* as well as of
138 genes involved in mitochondrial membrane and cristae organisation such as *Samm50*, (Figure
139 3C).

140 A recent body of evidence has revealed that stress responses, such as the integrated stress
141 response (ISR) or the closely related unfolded protein response (UPR), when triggered in cells
142 with impaired mitochondrial function prompt a transcriptional program to restore cellular

143 homeostasis (Melber and Haynes, 2018; Munch, 2018; Topf et al., 2016). We observed that loser
144 epiblast cells displayed a characteristic UPR-ISR signature (Figure S3A-C) (Mouchiroud et al.,
145 2013; Nargund et al., 2012; Quiros et al., 2016; Zhao et al., 2002) and key regulators of this
146 response, such as *Atf4, Ddit3*, *Nrf2* and *Foxo3* were all up-regulated in these cells (Figure S3D).
147 Similarly, *Sesn2*, a target of p53 that controls mTOR activity (Saveljeva et al., 2016), was also up-
148 regulated in loser cells (Figure S3D). These findings support the possibility that loser epiblast
149 cells present mitochondrial defects, leading to the activation of a stress response in an attempt to
150 restore cellular homeostasis (Yun and Finkel, 2014).

151 To validate the significance of the mitochondrial defects observed, we did two things. First, we
152 asked if the changes observed at the mRNA level are also reflected at the protein level. We
153 observed that in CI-treated embryos, loser cells that persist and are marked by low mTOR activity
154 (Bowling et al., 2018), also show significantly lower OPA1 levels (Figure 3D-F). This finding is in
155 agreement with the observation that OPA1 levels are decreased during mitochondrial stress
156 (Quiros et al., 2017). We also found that DMSO-treated embryos showed strong DDIT3 staining
157 (an UPR-ISR marker) in the dying cells that accumulate in the proamniotic cavity, and that in CI-
158 treated embryos, DDIT3 expression was up-regulated in a proportion of epiblast cells (Figure S3E-
159 G). The second thing we did to validate the importance of the mitochondrial defects observed was
160 to study in loser epiblast cells the mitochondrial membrane potential ($\Delta\psi m$), an indication of
161 mitochondrial health. We observed that while the cells of DMSO-treated embryos showed a high
162 $\Delta\psi m$ that fell within a narrow range, in CI-treated embryos the proportion of cells with a low $\Delta\psi m$
163 significantly increased (Figure 3D and 3G-H). Together, these results suggest that loser epiblast
164 cells have impaired mitochondrial activity that triggers a stress response.

165 **Mitochondrial dysfunction is common to different types of loser cells**

166 The above data indicate that loser epiblast cells are mis-patterned and show mitochondrial
167 defects. To address if mitochondrial defects are a common feature of mis-patterned cells we
168 analysed ESCs that are defective for BMP signalling (*Bmpr1a*$^{-/-}$), as these are abnormally
169 patterned (Di-Gregorio et al., 2007) and eliminated by cell competition (Sancho et al., 2013). In
170 parallel, to determine if mitochondrial defects are present in other loser cells eliminated by cell
171 competition, we also studied tetraploid cells (4n) (Sancho et al., 2013). We first carried out a mass
172 spectrometry analysis using the Metabolon platform and found that metabolites and intermediates
173 of the TCA cycle, such as malate, fumarate, glutamate and α-ketoglutarate are depleted in both
174 *Bmpr1a*$^{-/-}$ and 4n ESCs in differentiation culture conditions (Figure 4A). Next, we performed an
175 extracellular flux Seahorse analysis of *Bmpr1a*$^{-/-}$ ESCs to measure their glycolytic and oxidative
176 phosphorylation (OXPHOS) rates. We observed that when these cells are maintained in
177 pluripotency culture conditions, that are not permissive for cell competition (Sancho *et al.*, 2013),
178 they showed a similar glycolytic activity, but a higher OXPHOS rate than control cells (Figure S4A-

179 D). In contrast, when *Bmpr1a*$^{-/-}$ cells are induced to differentiate, this phenotype is reversed, with
180 mutant cells showing lower ATP generated through OXPHOS and a higher glycolytic capacity than
181 controls (Figure 4B-E; Figure S4E-F). This suggests that upon differentiation *Bmpr1a*$^{-/-}$ cells are
182 unable to sustain proper OXPHOS activity.

183 To further test the possibility that defective ESCs have impaired mitochondrial function, we
184 assessed their Δψm. We found that whilst *Bmpr1a*$^{-/-}$ and 4n cells had a similar Δψm to control cells
185 in pluripotency conditions (Figure S4G-H), upon differentiation both these cell types presented a
186 loss of Δψm, irrespective of whether they were separate or co-cultured with wild-type cells (Figure
187 4F-G). This reduction in Δψm is unlikely to be due to excessive mitochondrial reactive oxygen
188 species (ROS) production or to a lower mitochondrial mass within mutant cells since, as for
189 example, *Bmpr1a*$^{-/-}$ cells have lower ROS levels and similar TOMM20 and mt-CO1 expression as
190 control cells (Figure 4H-J; Figure S4I). The fact that the loss of Δψm and lower OXPHOS activity
191 can be observed even when loser cells are cultured separately, suggests that the mitochondrial
192 dysfunction phenotype is an inherent property of loser cells and not a response to them being out-
193 competed. These results also indicate that the mitochondrial defects are directly linked to the
194 emergence of the loser status: in conditions that are not permissive for cell competition
195 (pluripotency) mutant cells do not show defective mitochondrial function, but when they are
196 switched to differentiation conditions that allow for cell competition, they display impaired
197 mitochondrial function.

198 To further explore the relationship between mitochondrial activity and the competitive ability of the
199 cell, we analysed the Δψm of BMP defective cells that are null for p53 (*Bmpr1a*$^{-/-}$*; p53*$^{-/-}$ ESCs), as
200 these are not eliminated by wild-type cells (Bowling et al., 2018). Remarkably, we observed that
201 mutating *p53* in *Bmpr1a*$^{-/-}$ cells not only rescues the loss of Δψm of these cells, but also causes
202 hyperpolarisation of their mitochondria (Figure 4K). These results strongly support a pivotal role
203 for mitochondrial activity in cell competition.

204 Impaired mitochondrial function is sufficient to trigger cell competition

205 The mitochondrial defects observed in loser cells led us to ask if disrupting mitochondrial activity
206 alone is sufficient to trigger cell competition. During the onset of differentiation, mitochondria go
207 from having a fragmented shape to fusing and forming complex networks (reviewed in (Lima et
208 al., 2018). We therefore tested if disrupting mitochondrial dynamics induces cell competition.
209 MFN1 and MFN2 regulate mitochondrial fusion and DRP1 controls their fission (Chen et al., 2003;
210 Prudent and McBride, 2017; Smirnova et al., 2001). We generated *Drp1*$^{-/-}$ ESCs, that show hyper-
211 elongated mitochondria, and *Mfn2*$^{-/-}$ ESCs, that have enlarged globular mitochondria (Figure 5A).
212 Analysis of the *Drp1* mutant cells showed that although they did not grow significantly slower than
213 wild-type cells when cultured separately in differentiation inducing conditions, they were out-

214 competed by wild-type cells in co-culture (Figure 5B). In contrast to this, we observed that *Mfn2*$^{-/-}$
215 ESCs displayed very poor growth upon differentiation (data not shown). For this reason, we tested
216 their competitive ability in pluripotency conditions, that we have previously found not to induce the
217 out-competition of *Bmpr1a*$^{-/-}$ or 4n cells (Sancho et al., 2013). Interestingly, we found that although
218 *Mfn2*$^{-/-}$ cells grow similarly to wild-type cells in separate cultures, they were out-competed in co-
219 culture (Figure 5C). The observation that disrupting mitochondrial dynamics can induce cell
220 competition even in pluripotency culture conditions, suggests that mitochondrial activity is a
221 dominant parameter determining the competitive ability of the cell.

222 Loser epiblast cells accumulate mtDNA mutations

223 There is strong evidence for selection against aberrant mitochondrial function induced by
224 deleterious mtDNA mutations in mammals (Fan et al., 2008; Freyer et al., 2012; Kauppila et al.,
225 2016; Sharpley et al., 2012; Stewart et al., 2008). Given that we observe that cell competition
226 selects against cells with impaired mitochondrial function, we asked if cell competition could be
227 reducing mtDNA heteroplasmy (frequency of different mtDNA variants) during mouse
228 development. It has been recently shown that scRNA-seq can be used to reliably identify mtDNA
229 variants, although with a lower statistical power compared to more direct approaches, like mtDNA
230 sequencing (Ludwig et al., 2019). We therefore tested if mtDNA heteroplasmy is present in our
231 scRNA-seq data and whether this is associated with the losing score of a cell. Our analysis
232 revealed that the frequency of specific mtDNA polymorphisms increased with the losing score of
233 epiblast cells (Figure 6A), and such mtDNA changes occurred within *mt-Rnr1* and *mt-Rnr2* (Figure
234 6B-H and Figure S5A-E). Moreover, these changes were not dependant on the litter from which
235 the embryo came from (Figure S5F-K). The mutations we detected in *mt-Rnr1* and *mt-Rnr2*
236 strongly co-occurred in the same cell, with those closest together having the highest probability of
237 co-existing (Figure 6I and Figure S5L). This is suggestive of mtDNA replication errors that could
238 be 'scarring' the mtDNA, disrupting the function of *mt-Rnr1* (12S rRNA) and *mt-Rnr2* (16S rRNA)
239 and causing the loser phenotype. Importantly, the presence of these specific mtDNA mutations in
240 the loser cells suggests that cell competition is contributing to the elimination of deleterious mtDNA
241 mutations during early mouse development.

242 Changes in mtDNA sequence can determine the competitive ability of a cell

243 To explore this possibility further we analysed if alterations in mtDNA can induce cell competition
244 by testing the competitive ability of ESCs with non-pathological differences in mtDNA sequence.
245 For this we compared the relative competitive ability of ESCs that shared the same nuclear
246 genome background but differed in their mitochondrial genomes by a small number of non-
247 pathological sequence changes. We derived ESCs from hybrid mouse strains that we had
248 previously engineered to have a common nuclear C57BL/6N background, but mtDNAs from

249 different wild-caught mice (Burgstaller et al., 2014). Each wild-derived mtDNA variant (or
250 haplotype) contains a specific number of single nucleotide polymorphisms (SNPs) that lead to a
251 small number of amino acid changes when compared to the C57BL/6N mtDNA haplotype.
252 Furthermore, these haplotypes (BG, HB and ST) can be ranked according to their genetic distance
253 from the C57BL/6N mtDNA (Figures 7A and S6A). Characterization of the isolated ESCs revealed
254 that they have a range of heteroplasmy (mix of wild-derived and C57BL/6N mtDNAs) that is stable
255 over several passages (Figure S6B). Importantly, these different mtDNA haplotypes and different
256 levels of heteroplasmy do not alter cell size, cell granularity, mitochondrial mass or mitochondrial
257 dynamics, nor do they substantially impact the cell's $\Delta\psi m$ (Figure S6C-F).

258 When we tested the competitive ability of these mtDNA ESCs we observed that cells carrying the
259 mtDNAs that are most distant from the C57BL/6N mtDNA, such as the HB(100%), the HB(24%)
260 and the ST(46%) ESCs could all out-compete the C57BL/6N line (Figure 7B-C and S6G).
261 Similarly, when we tested the HB(24%) line against the BG(99%) or the BG(95%) lines (that have
262 mtDNAs more closely related to the C57BL/6N mtDNA), we found that cells with the HB haplotype
263 could also out-compete these ESCs (Figure 7D and S6H). In contrast, we observed that the
264 HB(24%) ESCs were unable to out-compete either their homoplasmic counterparts, HB(100%),
265 or the ST(46%) cells that carry the most distant mtDNA from C57BL/6N (Figure 7E and S6I).
266 These results tell us three things. First, that non-pathological differences in mtDNA sequence can
267 trigger cell competition. Second, that a competitive advantage can be conferred by only a small
268 proportion of mtDNA content, as indicated by our finding that HB(24%) behave as winners. Finally,
269 these findings suggest that the phylogenetic proximity between mtDNA variants can potentially
270 determine their competitive cell fitness.

271 To characterise the mode of competition between different mtDNA cells we focussed on the
272 HB(24%) and the BG(95%) ESCs. Analysis of these cell lines revealed that specifically when co-
273 cultured, the BG(95%) cells display high levels of apoptosis (Figure 7F), indicating that their out-
274 competition is through their elimination. To gain further insight we performed bulk RNA-seq of
275 these cells in separate and co-culture conditions (Figure S6J) and analysed the differentially
276 expressed genes by gene-set enrichment analysis (GSEA). We found that in separate culture the
277 most notable features that distinguish BG(95%) from HB(24%) cells were a down-regulation of
278 genes involved in oxidative phosphorylation and an up-regulation of those associated with
279 cytokine activity (Figure 7G). Interestingly, in the co-culture condition, in addition to these
280 signatures, BG(95%) cells revealed a down-regulation in signature markers of MYC activity and
281 mTOR signalling (Figure 7H), whose downregulation are known read-outs of a loser status during
282 cell competition in the embryo (Bowling et al., 2018; Claveria et al., 2013; Sancho et al.,
283 2013)(Figure 2C). These results suggest that the elimination of loser mtDNA cells occurs through
284 the same mechanism as the out-competition of defective cells in the embryo (Figure 7I).

285 The finding that the genes down-regulated in BG(95%) cells when co-cultured with HB(24%) cells
286 fell under functional categories relating to mitochondrial function (Figure S7A) led us to analyse
287 the degree of overlap between these genes and the genes differentially expressed along the
288 winner-to-loser trajectory in the embryo. We observed a significant overlap in down-regulated
289 genes (Figure S7B), as well as in the functional components that these genes can be categorised
290 into (Figure S7C). This further highlights the importance of relative mitochondrial activity for
291 determining the competitive ability of embryonic cells.

292 Discussion

293 The emerging role of cell competition as a regulator of cell fitness in a wide range of cellular
294 contexts, from the developing embryo to the ageing tissue (reviewed in (Bowling et al., 2019; Diaz-
295 Diaz and Torres, 2019; Madan et al., 2018), has highlighted the importance of understanding what
296 cell types are normally eliminated by this process. With the aim of understanding this question,
297 we have analysed the transcriptional identity of the cells eliminated in the early mouse embryo.
298 We have found not only that they present a cell competition signature, but also that they are mis-
299 patterned and marked by impaired mitochondrial function. Starting from these results, we
300 leveraged *in vitro* models of cell competition to show that: (i) mitochondrial function is impaired in
301 loser cells eliminated by cell competition, and (ii) that differences in mitochondrial activity are
302 sufficient to trigger cell competition in ESCs. Overall, this points to mitochondrial performance as
303 a key determinant of the competitive ability of cells during early mammalian embryonic
304 development. One implication of our findings is that a range of different types of defect, such as
305 mis-patterning, karyotypic abnormalities or mtDNA mutations, all lead to dysfunctional
306 mitochondria at the onset of differentiation and that ultimately it is their impaired mitochondrial
307 function that triggers cell competition, inducing their elimination (Figure 7I).

308 It is well known that the successful development of the embryo can be influenced by the quality of
309 its mitochondrial pool (reviewed in (Lima et al., 2018). Moreover, divergence from normal
310 mitochondrial function during embryogenesis is either lethal or can lead to the development of
311 mitochondrial disorders (Chinnery and Hudson, 2013). Deleterious mtDNA mutations are a
312 common cause of mitochondrial diseases and during development selection against mutant
313 mtDNA has been described to occur through at least through two mechanisms, the bottleneck
314 effect and intra-cellular purifying selection. The bottleneck effect is associated specifically with the
315 unequal segregation of mtDNAs during primordial germ cell specification, for example as seen in
316 the human embryo (Floros et al., 2018). In contrast to this, purifying selection, as the name implies,
317 allows for selection against deleterious mtDNAs and has been proposed to take place both during
318 development and post-natal life (Burr et al., 2018). Importantly, purifying selection has been found
319 to occur not only at the organelle level, but also at the cellular level (Rajasimha et al., 2008). Our

findings indicate that purifying selection can occur not only at the intra-cellular level but also inter-cellularly (cell non-autonomously). We show that epiblast cells are able to sense their relative mitochondrial activity and that those cells with mtDNA mutations, lower or aberrant mitochondrial function are eliminated. By selecting those cells with the most optimised mitochondrial performance, cell competition would not only prevent cells with mitochondrial defects from contributing to the germline or future embryo, but also ensure optimization of the bioenergetic performance of the epiblast, contributing to the synchronization of growth during early development.

Cell competition has been studied in a variety of organisms, from *Drosophila* to mammals, and it is likely that multiple different mechanisms fall under its broad umbrella (reviewed in (Bowling et al., 2019; Diaz-Diaz and Torres, 2019; Madan et al., 2018). In spite of this, there is considerable interest in understanding if there could be any common feature in at least some of the contexts where cell competition has been described. The first demonstration of cell competition in *Drosophila* was made by inducing clones carrying mutations in the ribosomal gene *Minute* (Morata and Ripoll, 1975) and this has become one of the primary models to study this process. Our finding that that during normal early mouse development cell competition eliminates cells carrying mutations in *mt-Rnr1* and *mt-Rnr2*, demonstrates that in the physiological context mutations in ribosomal genes also trigger cell competition. Furthermore, our observation that mis-patterned and karyotypically abnormal cells show impaired mitochondrial activity indicates that during early mouse development different types of defects impair mitochondrial function and trigger cell competition. Interestingly, mtDNA genes are amongst the top mis-regulated factors identified during cell competition in the mouse skin (Ellis et al., 2019). In the *Drosophila* wing disc oxidative stress, a general consequence of dysfunctional mitochondria, underlies the out-competition of *Minute* and *Mah-jong* mutant cells (Kucinski et al., 2017). Similarly, in Madin-Darby Canine Kidney (MDCK) cells, a loss of $\Delta\psi m$ occurs during the out-competition of RasV12 mutant cells and is key for their extrusion (Kon et al., 2017). These observations raise that possibility that differences in mitochondrial activity may be a key determinant of competitive cell fitness in a wide range of systems. Unravelling what mitochondrial features can lead to cellular differences that can be read between cells during cell competition will be key not only for understanding this process, but also to open up the possibility for future therapeutic avenues in the diagnosis or prevention of mitochondrial diseases.

Acknowledgments

We would like to thank Stephen Rothery for guidance and advice with confocal microscopy. Gratitude also goes to James Elliot and Bhavik Patel for performing cell sorts. Research in Tristan Rodriguez lab was supported by the MRC project grant (MR/N009371/1) and by the British Heart

Foundation centre for research excellence. Ana Lima was funded by a BHF centre of excellence PhD studentship. Shankar Srinivas was funded through Wellcome awards 103788/Z/14/Z and 108438/Z/15/Z.

Author Contributions

A.L. performed most of the experimental wet lab work. J.B. and A.L. derived heteroplasmic mESC lines. J.B. performed heteroplasmy measurements in heteroplasmic mESCs. B.P. generated *Mfn2*$^{-/-}$ and *Drp1*$^{-/-}$ mESCs and J.M.S did characterisation of mitochondria shape and pluripotency status. D.H. performed embryo dissections, treatments and cell dissociation prior to scRNA-seq experiments. G.L. did the bioinformatic analysis of scRNA-seq data. E.M., N.J. and A.G. participated in the analysis of mitochondrial DNA heteroplasmy. A.D.G. performed the metabolomic studies using Metabolon platform and participated in embryo dissections and immunohistochemistry stainings for validation of results obtained by scRNA-seq. M.D, and M.K. performed the bioinformatic analysis of bulk RNA-seq experiments. N.J., S.S. and D.C. participated in the design of experimental work and analysis of results. A.L., G.L., A.S and T.R. interpreted results and wrote the paper. T.R. and A.S. directed and designed the research.

Declaration of Interests

The authors declare no competing interests.

372 # Figure titles and legends

373 **Figure 1. Cells eliminated during early mouse embryogenesis have a distinct**
374 **transcriptional profile.**
375 (A) Experimental design. The number of cells in the two conditions (DMSO-treated and CI-treated)
376 refers to the number of cells that passed the quality control.
377 (B) Identification of the clusters according to known gene markers from the different embryonic
378 regions. Three clusters (clusters 1, 3 and 4) show marker genes of the epiblast (Epi), while the
379 remaining clusters correspond to the extra-embryonic lineages visceral endoderm (VE; cluster 5)
380 and extraembryonic ectoderm (ExE; cluster 2). The epiblast clusters are named "Winner",
381 "Intermediate" and "Loser" on the basis of the relative fraction of cells from CI-treated embryos
382 they include (see panel E).
383 (C-D) UMAP visualization of the single-cell RNA-seq data, with cells coloured according to cluster
384 (C) or condition (D). A region made up exclusively by cells from CI-treated embryos emerges.
385 (E) Ratio between the fraction of cells from DMSO-treated and CI-treated embryos in the three
386 epiblast clusters. While the "winner" epiblast cluster shows an enrichment of cells from DMSO-
387 treated embryos, the "intermediate" and the "loser" epiblast clusters are strongly enriched for cells
388 from CI-treated embryos.
389 See also Figure S1

390 **Figure 2. A cell competition transcriptional signature is identified in cells eliminated during**
391 **mouse embryonic development**
392 (A) Diffusion map of epiblast cells (only from CI-treated embryos), coloured by cluster.
393 (B-C) IPA run on the list of genes differentially expressed along the diffusion trajectory (see Figure
394 S2D) generated lists of top 5 molecular and cellular functions (B) and upstream regulators (C)
395 found to be differentially activated in epiblast cells along the diffusion trajectory from winner
396 (cluster 1) to loser status (cluster 4).
397 (D) Diffusion map of epiblast cells (only from CI-treated embryos) colored by diffusion pseudotime
398 coordinate (dpt). The winner and the loser clusters are found at the two extremities of the
399 trajectory, hence the dpt can be interpreted as a "losing score".
400 (E) Losing score of the cells in the three epiblast clusters in CI-treated (left) or DMSO-treated
401 (right) embryos. The losing score of the cells from DMSO-treated embryos was obtained by
402 projecting them on the diffusion map shown in panel D (see Methods).
403 (F) Expression levels of genes (in rows) that are markers for naïve pluripotency (*Klf4* and *Klf5*),
404 primed pluripotency (*Fgf5* and *Tdgf1*), mesoderm (*Mesp1* and *T*), neuroectoderm (*Neurod1* and
405 *Sox1*) and endoderm (*Sox17*). Cells (in columns) are sorted by their losing scores. The genes
406 marked with a * are differentially expressed along the trajectory.

407 (G) Scatter plots of the expression levels of different marker genes in cells from the loser epiblast
408 cells (cluster 4), suggesting that loser cells are mis-patterned.
409 See also Figure S2.

410 **Figure 3. Cells eliminated during early mouse embryogenesis have mitochondrial defects.**
411 (A) Top canonical pathways, identified by IPA, mis-regulated in loser cells in comparison to normal
412 epiblast cells. The numbers at the end of each bar refer to total amount of genes involved in that
413 pathway. The percentage refers to the number of genes found mis-regulated relative to the
414 number total genes within each pathway. Statistical significance calculated with Fisher's exact test
415 ($p<0.05$): Mitochondrial Dysfunction, -log10(p-value) = 21.1; Oxidative Phosphorylation, - log10(p-
416 value) = 18.6; EIF2 signalling, - log10(p-value) = 11.9.
417 (B) Detail of changes in oxidative phosphorylation pathway identified in (A). Circular and oval
418 shapes represent each of the ETC complexes (complexes I to V). Diamond shapes represent
419 subunits of each ETC complex. Genes that are differentially expressed between loser and winner
420 epiblast cells are colored in shades of red, with darker shades corresponding to lower values of
421 FDR, which ranges from 1.25E-51 (for *Atp5b*) to 5.42E-03 (for *Ndufa11*). Grey color denotes
422 genes that were not significant (FDR>0.01). White color denotes genes from the Knowledge Base
423 that were not tested (e.g., because they were not detected in our dataset).
424 (C) Expression levels of some mitochondrial genes as a function of cells' losing score. *mt-Atp6*,
425 mitochondrial DNA encoded ATP synthase membrane subunit 6; *mt-Nd3*, mitochondrial DNA
426 encoded NADH dehydrogenase subunit 3; *Opa1*, optic atrophy 1; *Samm50*, sorting and assembly
427 machinery component 50 homolog.
428 (D) Experimental design adopted to assess mitochondria function (OPA1 expression, by
429 immunofluorescence or Δψm, given by TMRM fluorescence) in epiblast cells from embryos where
430 cell death was allowed (DMSO-treated) or inhibited (CI-treated). * Micrograph of isolated epiblast
431 (arrow) after embryo microdissection.
432 (E) Representative immunohistochemistry of OPA1 in E6.5 embryo where cell death was inhibited
433 (CI-treated), quantified in (F). Loser cells are identified by low mTOR activation (low p-rpS6,
434 arrowheads). Scale bar = 20 μm.
435 (F) Quantification of OPA1 fluorescence in normal epiblast cells and loser cells. N=6 embryos with
436 a minimum of 8 cells analysed per condition. Statistical analysis performed by Mann-Whitney test.
437 (G) Representative histogram of flow cytometry analysis of TMRM probe, indicative of Δψm, in
438 epiblast cells from embryos where cell death was allowed (DMSO-treated) or inhibited (CI-
439 treated), quantified in (H).
440 (H) Frequency of epiblast cells with high or low TMRM fluorescence, according to range defined
441 in (G) from embryos where cell competition was allowed (DMSO treated) or inhibited (CI-treated).
442 Statistical analysis done by two-way ANOVA, followed by Holm-Sidak's multiple comparisons test.

443 N=3 independent experiments. Data shown as mean ± SEM.
444 See also Figure S3.

445 **Figure 4. Mitochondrial defects are a common feature of cells eliminated by cell**
446 **competition.**
447 (A) Metabolic enrichment analysis of the TCA cycle and intermediate metabolites obtained using
448 Metabolon platform for defective cells (*Bmpr1a*$^{-/-}$, left bar and 4n, right bar), in comparison to wild-
449 type cells during differentiation. Bars indicate compound levels relative to wild-type cells. Blue bars
450 indicate compounds that are significantly depleted ($p<0.05$) and light blue bars indicate
451 compounds that are almost significantly depleted ($0.05 \leq p \leq 0.1$). Black bars indicate compounds
452 that are depleted although not statistically significant in comparison to the levels found in wild-type
453 cells. The enzymes on the pathway are represented as boxes and labelled by their canonical
454 names.
455 (B-E) Metabolic flux analysis of wild-type and BMP-defective cells during differentiating conditions.
456 Statistical analysis done with Mann-Whitney test. Analysis of oxygen consumption rate (OCR) as
457 a measure of mitochondria function (mitochondria stress test) (B). Detail of metabolic parameters
458 found changed from the analysis of the mitochondria stress test (C). Analysis of extracellular
459 acidification rate (ECAR) as a measure of glycolytic function (glycolysis stress test) (D). Detail of
460 metabolic parameters found changed from the analysis of the glycolysis stress test (E).
461 (F-G) Analysis of mitochondrial membrane potential (Δψm) in defective mESCs undergoing
462 differentiation in separate or co-culture conditions. Representative histograms of TMRM
463 fluorescence and quantification for wild-type and *Bmpr1a*$^{-/-}$ (F) and wild-type and 4n (G). Statistical
464 analysis done by two-way ANOVA, followed by Holm-Sidak's multiple comparisons test.
465 (H) Representative micrographs of wild-type and *Bmpr1a*$^{-/-}$ cells co-cultured during differentiation
466 and stained for marker of Δψm (MitoTracker Red, top panel) or mitochondria mass (TOMM20,
467 bottom panel). Nuclei are stained with Hoechst. Scale bar = 10 μm.
468 (I-J) Western blot analysis of mitochondria mass markers TOMM20 (I) and mt-CO1 (J) for wild-
469 type and *Bmpr1a*$^{-/-}$ cells during differentiation. Statistical analysis done with Mann-Whitney test.
470 (K) Analysis of mitochondrial membrane potential (Δψm) for wild-type, *Bmpr1a*$^{-/-}$ and *Bmpr1a*$^{-/-}$
471 ;*p53*$^{-/-}$ cells during differentiation. Representative histogram of TMRM fluorescence and
472 quantification. Statistical analysis done by one-way ANOVA, followed by Holm-Sidak's multiple
473 comparisons test.
474 Data shown as mean ± SEM of a minimum of 3 independent experiments.
475 See also Figure S4.

476 **Figure 5. Manipulating mitochondria biology is sufficient to trigger cell competition.**

477 (A) Representative micrographs of wild-type, *Drp1*$^{-/-}$ and *Mfn2*$^{-/-}$ mESCs showing alterations in
478 mitochondrial morphology in mutant cells. TOMM20 was used as mitochondrial marker and
479 NANOG as a pluripotency marker. Nuclei are stained with Hoechst. Scale bar = 5 µm.
480 (B-C) Cell competition assays between wildtype mESCs and cells with altered morphology, *Drp1*$^{-}$
481 $^{/-}$ (B) and *Mfn2*$^{-/-}$ (C). The ratio of final/initial cell numbers in separate or co-culture is shown.
482 Statistical analysis done with two-way ANOVA, followed by Holm-Sidak's multiple comparisons
483 test.

484 **Figure 6. Intermediate and loser epiblast cells accumulate polymorphisms in mtDNA**
485 **sequence.**
486 (A-G) mtDNA heteroplasmy, *H*, in epiblast cells from CI-treated embryos. Average heteroplasmy
487 (considering all eleven polymorphisms that have a statistically significant dependence on the
488 losing score; see Methods) as a function of cells' losing scores. The p-value was computed with
489 a generalized linear model (A). mtDNA heteroplasmy for six positions within the *mt-Rnr1* gene (B-
490 G). The heteroplasmy at all of these positions as well as the average heteroplasmy increase with
491 the cells' losing scores in a statistically significant way (the adjusted p-value estimated via a
492 generalized linear model is indicated at the top of each plot).
493 (H) The barplot indicates the fraction of epiblast cells in each of the cluster indicated on the x-axis
494 (winner, intermediate, loser) that carry a mean heteroplasmy *H (*computed on the six positions
495 within the *mt-Rnr1* indicated in the panels B-G) greater than 0.01. This shows that the level of
496 mtDNA heteroplasmy in *mt-Rnr1* is strongly associated with the loser status of the cells, since
497 ~55% and ~87% of cells in the intermediate and the loser clusters, respectively, have
498 heteroplasmic sequences in this gene compared to only ~5% of cells in the winner cluster.
499 (I) Spearman's correlation coefficient between the mtDNA heteroplasmy at the six positions shown
500 in panels (B-G).
501 See also Figure S5.

502 **Figure 7. Changes in mtDNA sequence can determine the competitive ability of a cell.**
503 (A) Derivation of mESCs from hybrid mouse strains, generated elsewhere by Burgstaller and
504 colleagues. Neighbour-Joining Phylogenetic Analysis of mtDNA from wild and C57BL/6N mouse
505 strains, that were used to generate hybrid mice (adapted from Burgstaller et al, 2014), illustrates
506 the genetic distance of the mtDNA from wild mouse strains to the C57BL/6N lab mouse. The
507 number of single nucleotide polymorphisms and amino acid changes (SNPs/ a.a. changes) from
508 wild to lab mouse strain is shown. mESCs were derived from embryos of hybrid mice, containing
509 the nuclear background of a C57BL/6N lab mouse and mtDNA from three possible wild-derived
510 strains (BG, HB or ST).

511 (B-E) Cell competition assays between cells derived from the embryos of hybrid mice. The ratio
512 of final/initial cell numbers in separate or co-culture is shown. Statistical analysis done with two-
513 way ANOVA, followed by Holm-Sidak's multiple comparisons test.
514 (F) Representative micrographs of cleaved caspase-3 staining and quantification of the
515 percentage of apoptotic events in winners HB(24%) and loser BG(95%) mESCs and cultured in
516 separate or co-culture conditions. Statistical analysis done with two-way ANOVA, followed by
517 Holm-Sidak's multiple comparisons test.
518 (G-H) Gene set enrichment analysis of differentially expressed genes from bulk RNA seq. in loser
519 loser BG (95%) compared to winner HB (24%) mESCs cultured in separate (J) or co-culture
520 conditions (K). Gene sets that show positive normalized enrichment scores (NES) are enriched in
521 loser cells, while gene sets that show negative NES are depleted in loser cells.
522 (I) Summary of the main findings of the study. A range of cellular defects, such as aneuploidy,
523 mis-patterning or mtDNA mutations cause alterations in mitochondria function, which affect the
524 relative fitness of cells. The cells with suboptimal mitochondrial activity survive in a homogeneous
525 population, but are eliminated by cell competition in the presence of fitter cells.
526 Data in panels (B-F) shown as mean ± SEM of a minimum of 3 independent experiments.
527 See also Figure S6.

528 **Figure S1. Quality controls of scRNA-seq**
529 (A) These boxplots show the log10-total number of reads (top left), the fraction of mapped reads
530 (top central), the fraction of reads mapped to endogenous genes (top right), the fraction of reads
531 mapped to mitochondrial genes (bottom left), the fraction of reads mapped to ERCC spike-ins
532 (bottom central) and the number of genes with more than 10 reads per million (bottom right) for all
533 cells (723) that passed the quality control.
534 (B) Number of good quality cells in each condition (rows) and batch (columns).
535 (C) Number of good quality cells per cluster (rows) and batch (columns).
536 (D) UMAP plot of the data with cells colored by batch. In each batch there is a balanced
537 distribution of cells in the two conditions and across the five clusters.

538 **Figure S2. Analysis on epiblast cells from DMSO and CI-treated embryos**
539 (A-B) Diffusion map analysis in all epiblast cells (from DMSO and CI-treated embryos): cells are
540 coloured according to the condition (A) and to the cluster (B).
541 (C) The pseudo-time coordinate of the CI-treated epiblast cells obtained from the diffusion map
542 including all epiblast cells correlates extremely well with the pseudo-time coordinate obtained in
543 the diffusion map calculated only from CI-treated epiblast cells (Figure 2A).
544 (D) Heatmap showing the expression pattern of all genes differentially expressed along the
545 trajectory from winning to losing cells in Figure 2D.

546 (E-F) Overlap of genes differentially expressed along the trajectory joining winning and losing
547 epiblast cells in CI-treated embryos (Figure 2A and S2D) and genes targeted by p53. Pie charts
548 show the percentage of genes up- or down-regulated in loser cells within the group of target genes
549 that are activated (E) or repressed (F) by p53. There is an enrichment of activated/repressed
550 targets among genes upregulated/downregulated in losing cells respectively (Fisher's test, p-
551 value=1E-4). The list of p53 targets is taken from (Fischer, 2017).

552 **Figure S3. Cells eliminated during early mouse embryogenesis have activated stress**
553 **responses.**
554 (A) Overlap of genes differentially expressed along the trajectory joining winning and losing
555 epiblast cells in CI-treated embryos (Figure 2A and Figure S2F) and genes related to the unfolded
556 protein response and integrated protein response pathways (UPR_ISR, see Supplementary Table
557 3). From the 32 genes related to the UPR & ISR pathways, 12 are down-regulated in loser cells,
558 8 genes are up-regulated in loser cells, and 12 genes are not differentially expressed between
559 loser and winner cells. There is a statistically significant enrichment of UPR&ISR genes among
560 the up-regulated genes in loser cells (Fisher test, odds ratio=3.0, p-value=0.012). The intersection
561 between UPR-ISR genes and the down regulated genes is not significant (Fisher test, odds
562 ratio=1.2, p value=0.69).
563 (B-C) List of genes from UPR-ISR pathways that are statistically significantly upregulated (B) or
564 downregulated (C) in loser cells.
565 (D) Scatterplots with the expression levels of genes involved in stress responses in epiblast cells
566 from CI-treated embryos as a function of cells' losing score.
567 (E) Experimental design with the approach taken to validate the expression of the stress response
568 marker DDIT3 in epiblast cells from DMSO or CI-treated embryos.
569 (F) Representative micrographs of DMSO (upper panel) or CI-treated embryos (100 μM, lower
570 panel) stained for DDIT3, quantified in (G). Nuclei are labelled with Hoechst. In control embryos
571 (DMSO-treated), dying cells in the cavity show very high DDIT3 expression (arrow), while live cells
572 in the epiblast of the CI-treated embryos show more modest levels of DDIT3 expression
573 (arrowheads). Scale bar = 20 μm.
574 (G) Quantification of the percentage of epiblast cells with nuclear DDIT3 expression. N=10 DMSO
575 and N=9 CI-treated embryos. Data shown as mean ± SEM.
576 *Ddit3 (Chop)*, DNA-damage inducible transcript 3; *Atf3*, activating transcription factor 3; *Atf4*,
577 activating transcription factor 4; *Foxo3*, forkhead box O3; *Ppp1r115a (Gadd34),* Protein
578 Phosphatase 1 Regulatory Subunit 15A, *Eif2ak3 (Perk),* Eukaryotic Translation Initiation Factor 2
579 Alpha Kinase 3; *Nfe2l2 (Nrf2)*, NFE2-related factor 2;. *Sesn2*, Sestrin 2; *Gdf15*, Growth
580 Differentiation Factor 15; *Mthfd1l*, Methylenetetrahydrofolate Dehydrogenase (NADP+
581 Dependent) 1 Like; *Hspe1*, Heat Shock Protein Family E (*Hsp10*) Member 1; *Cat*, Catalase;

582 *Hspd1*, Heat Shock Protein Family D (Hsp60) Member 1; *Sod2,* Superoxide Dismutase 2; *Hsph1,*
583 Heat Shock Protein Family H (*Hsp110*) Member 1; *Lonp1*, Lon Peptidase 1, Mitochondrial; *Eif2a,*
584 Eukaryotic Translation Initiation Factor 2A; *Mthfd2*, Methylenetetrahydrofolate Dehydrogenase
585 (NADP+ Dependent) 2, Methenyltetrahydrofolate Cyclohydrolase; *Hspa4*, Heat Shock Protein
586 Family A (*Hsp70*) Member 4; *Cth*, Cystathionine Gamma-Lyase; *Nrf1*, Nuclear Factor 1.

587 **Figure S4. Mitochondrial function in Wild-type, *Bmpr1a*$^{-/-}$ and 4n mESCs**
588 (A-F), Metabolic analysis of wild-type and *Bmpr1a*$^{-/-}$ mESCs. OCR profile during the mitochondria
589 stress test performed in pluripotency conditions (A). Metabolic parameters assessed during the
590 mitochondria stress test performed in pluripotency conditions (B). ECAR profile during the
591 glycolysis stress test performed in pluripotency conditions (C). Metabolic parameters assessed
592 during the glycolysis stress test performed in pluripotency conditions (D). Metabolic parameters
593 from the mitochondria stress test found to be similar between wild-type and *Bmpr1a*$^{-/-}$ mESCs
594 during differentiation (E). Metabolic parameters from the glycolysis stress test found to be similar
595 between wild-type and *Bmpr1a*$^{-/-}$ mESCs during differentiation (F).
596 (G-H) Analysis of mitochondrial membrane potential (Δψm) in defective mESCs maintained in
597 pluripotency conditions, in separate or co-culture. Representative histograms of TMRM
598 fluorescence and quantification for wild-type and *Bmpr1a*$^{-/-}$ (G) and wild-type and 4n (H). Statistical
599 analysis done by two-way ANOVA, followed by Holm-Sidak's multiple comparisons test.
600 (I) Analysis of mitochondrial ROS in wild-type and *Bmpr1a*$^{-/-}$ mESCs undergoing differentiation in
601 separate or co-culture: representative histograms of mitoSOX Red fluorescence and quantification
602 of the percentage of mitoSOX positive cells.
603 Data obtained with a minimum of 3 independent experiments. Error bars represent SEM.

604 **Figure S5. Analysis of SNPs in mtDNA in epiblast cells.**
605 (A-E) mtDNA heteroplasmy, *H*, in epiblast cells from CI-treated embryos for five positions within
606 the *mt-Rnr2* gene. All of these positions have an heteroplasmy that increases with the cells' losing
607 scores in a statistically significant way (the adjusted p-value estimated via a generalized linear
608 model is indicated at the top of each plot).
609 (F-K) The variation in the heteroplasmy across the CI-treated cells is not due to a batch effect for
610 the 6 significant positions within the *mt-Rnr1* gene.
611 (L) Spearman's correlation between the mtDNA heteroplasmy at all the statistically significant
612 positions (six within the gene mt-*Rnr1* and five within the gene mt-*Rnr2*).

613 **Figure S6. Changes in mtDNA sequence are enough to trigger cell competition.**
614 (A) Illustration of the process of derivation of the mESCs lines from mice that are hybrid between
615 the wild-caught strains (BG, HB or ST) and the lab mouse (C57BL/6N). These hybrid mice were
616 generated elsewhere (Burgstaller et al, 2014) by ooplasmic transfer: the zygote of a C57BL/6N

617 mouse was injected with ooplasm from a wild-caught mouse (orange, HB pictured). Therefore,
618 these hybrid mice contain the nuclear background of the C57BL/6N strain and the mtDNA of wild-
619 caught strain and potentially C57BL/6N mtDNA (heteroplasmic mice strains). mESCs lines were
620 derived from the hybrid mice and characterised.
621 (B-F) Characterisation of cell lines derived by flow cytometry in comparison to the wild-type cell
622 line used in previous experiments (E14, 129/Ola background). Heteroplasmy analysis of the
623 derived mESC lines from the hybrid mice, indicating the percentage of wild-derived mtDNA (B).
624 Cell granularity (internal complexity) given as median fluorescence intensity of SSc-A laser (C).
625 Cell size given as median fluorescence intensity of FSc-A laser (D). Analysis of the expression of
626 mitochondrial markers: representative western blot and quantification of markers of mitochondrial
627 mass (ATPB, mt-CO1 and TOMM20) and mitochondrial dynamics (DRP1, MFN1and MFN2),
628 relative to vinculin, in cells derived from hybrid mice (E). Representative histograms and
629 quantification of median TMRM fluorescence, indicative of Δψm, for the hybrid cell lines derived,
630 in comparison to the wild-type cell line used in previous experiments (E14, 129/Ola
631 background)(F). Statistical analysis done by one-way ANOVA, followed by Holm-Sidak's multiple
632 comparisons test.
633 (G-I) Cell competition assays between hybrid cell lines. The ratio of final/initial cell numbers in
634 separate or co-culture is shown. Statistical analysis done by two-way ANOVA, followed by Holm-
635 Sidak's multiple comparisons test.
636 (J) Experimental design for RNA-Seq and GSEA. The isolation of RNA from winner HB(24%) and
637 loser BG(95%) cells was performed after three days in separate or co-culture conditions, once
638 cells have been subjected to FACS to isolate the two populations form mixed cultures.
639 Data obtained with a minimum of 3 independent experiments. Error bars represent SEM.

640 **Figure S7. Common features of scRNA-seq and bulk RNA-seq datasets.**
641 (A) Terms significantly enriched among genes downregulated in BG(95%) (loser) ESCs *in vitro*
642 when co-cultured with HB(24%) cells. The loss of mitochondrial activity emerges as a common
643 feature between loser cells *in vivo* and *in vitro*. The gene enrichment analysis was performed
644 using g-profiler tool (see Methods).
645 (B) Intersection between differentially expressed genes along the trajectory from winning to losing
646 epiblast cells ("in_vivo_scRNA-seq"; Figure 2A and S2D) and genes differentially expressed
647 between co-cultured HB(24%) (winner) and BG(95%) (loser) ESCs ("in_vitro_bulk_RNA-seq").
648 "Up" and "Down" here refer to genes up- or down-regulated in loser cells. Fisher test for the
649 intersection between down-regulated genes from scRNA-seq (*in vivo*) and down-regulated genes
650 from bulk RNA-seq (*in vitro*): p-value, 1.71E-12; odds ratio 1.80. Fisher test for the intersection
651 between down-regulated genes from scRNA-seq (*in vivo*) and up-regulated genes from bulk RNA-
652 seq (*in vitro*): p-value, 5.20E-3; odds ratio 0.67. Fisher test for the intersection between up-

regulated genes from scRNA-seq (*in vivo*) and down-regulated genes from bulk RNA-seq (*in vitro*): Fisher test p-value, 4.87E-3; odds ratio 0.80.The intersection between up-regulated genes from sc-RNA-seq (*in vivo*) and up-regulated genes from bulk RNA-Seq (*in vitro*) is not statistically significant: Fisher test p-value: 0.30, odds ratio 1.14.

(C) Intersection between the significantly enriched terms in genes upregulated or downregulated in loser cells in the epiblast of CI-treated embryos ("*in_vivo*_scRNA-Seq") or in our *in vitro* model of competition between co-cultured HB(24%) (winner) and BG(95%) (loser) ESCs ("*in_vitro*_bulk_RNA-seq"). All the terms enriched among downregulated genes *in vitro* are also enriched *in vivo*.

List of Tables.

Supplementary Table 1. List of genes down-regulated along the winner-to-loser trajectory in the embryo.

Supplementary Table 2. List of genes up-regulated along the winner-to-loser trajectory in the embryo.

Supplementary Table 3. Genes related to the unfolded protein response and integrated protein response pathways (UPR_ISR) that were analysed in the genes differentially expressed along the winner-to-loser trajectory.

Supplementary Table 4. List of background genes for the winner-to-loser trajectory in the embryo.

Supplementary Table 5. List of genes down-regulated in BG(95%) cells when co-cultured with HB(24%) cells.

Supplementary Table 6. List of genes up-regulated in BG(95%) cells when co-cultured with HB(24%) cells.

Supplementary Table 7. List of background genes used for the analysis of genes differentially expressed between co-cultured BG(95%) and HB(24%) cells .

678 # STAR Methods

679 **KEY RESOURCES TABLE**

680 Presented in a separate file

681 **LEAD CONTACT AND MATERIALS AVAILABILITY**

682 Tristan Rodriguez: tristan.rodriguez@imperial.ac.uk and Antonio Scialdone
683 antonio.scialdone@helmholtz-muenchen.de

684 **EXPERIMENTAL MODEL AND SUBJECT DETAILS**

685 **Cell lines and cell culture routine**

686 E14, kindly provided by Prof A. Smith, from Cambridge University, were used as wild-type control
687 cells tdTomato-labelled or unlabelled. GFP-labelled or unlabelled cells defective for BMP
688 signalling (*Bmpr1a*$^{-/-}$), tetraploid cells (4n) and *Bmp1a*$^{-/-}$ null for p53 (*Bmpr1a*$^{-/-}$;*p53*$^{-/-}$) are described
689 elsewhere (Bowling et al., 2018; Sancho et al., 2013). Cells null for Dynamin-related protein 1
690 (*Drp1*$^{-/-}$) or Mitofusin 2 (*Mfn2*$^{-/-}$) were generated by CRISPR mutagenesis. Cells with different
691 mitochondrial DNA (mtDNA) content in the same nuclear background were derived from embryos
692 of hybrid mice, generated elsewhere (Burgstaller et al., 2014).

693 Cells were maintained pluripotent and cultured at 37ºC in 5% CO_2 in 25 cm^2 flasks (Nunc) coated
694 with 0.1% gelatin (Sigma) in DPBS. Growth media (ES media) consisted of GMEM supplemented
695 with 10% FCS, 1mM sodium pyruvate, 2 mM L-glutamine, 1X minimum essential media non-
696 essential amino-acids, 0.1 mM β-mercaptoethanol (all from Gibco) and 0.1% leukemia inhibitory
697 factor (LIF, produced and tested in the lab). Cells derived from hybrid mice (C57BL/6N nuclear
698 background) were maintained on 0.2% LIF. The growth media was changed daily, and cells were
699 split every 3 days.

700 **CRISPR mutagenesis**

701 Drp1 and Mfn2 knockout ESCs were generated by CRISPR-Cas9 mediated deletion of Drp1 exon
702 2 and Mfn2 exon 3 respectively. sgRNA guides flanking Drp1 exon 2 or Mfn2 exon 3 were cloned
703 into the PX459 vector (Addgene)(Ran et al., 2013): Drp1 exon 2 upstream sgRNA:
704 5' TGGAACGGTCACAGCTGCAC 3'; Drp1 exon 2 downstream sgRNA:
705 5' TGGTCGCTGAGTTTGAGGCC 3'; Mfn2 upstream sgRNA: 5' GTGGTATGACCAATCCCAGA
706 3'; Mfn2 downstream sgRNA: 5' GGCCGGCCACTCTGCACCTT 3'. E14 ESCs were co-
707 transfected with 1ug of each sgRNA expression using Lipofectamine 2000 (Invitrogen) according
708 to manufacturer's instructions. As control E14 ESCs were transfected in parallel with equal amount
709 of empty PX459 plasmid. Following 6 days of Puromycin selection, single colonies were picked
710 from both Drp1 sgRNA and empty vector transfected ESCs and screened for mutations. Drp1
711 exon 2 deletion was confirmed by PCR genotyping using the following primers: Drp1_genot F: 5'
712 GGATACCCCAAGATTTCTGGA 3'; Drp1_genot R: 5' AGTCAGGTAATCGGGAGGAAA 3',

713 followed by Sanger Sequencing. Mfn2 exon 3 deletion was confirmed by PCR genotyping using
714 the following primers: Mfn2_genot F: 5' CAGCCCAGACATTGTTGCTTA 3'; Mfn2_genot R: 5'
715 AGCTGCCTCTCAGGAAATGAG 3', followed by Sanger Sequencing.

716 **Derivation of mESCs from hybrid mouse strains**

717 The derivation of new mESC lines was adapted from (Czechanski et al., 2014). Heteroplasmic
718 mESCs were derived from embryos of hybrid mouse strains BG, HB and ST. These contain the
719 mtDNA of C57BL/6N (Bl6) lab mouse and mtDNA variants from wild-caught mice (Burgstaller et
720 al., 2014).

721 Embryos were isolated at E2.5 (morula stage) and cultured in 4-well plates (Nunc, Thermo
722 Scientific) containing KSOM media (Millipore) plus two inhibitors (KSOM+2i): 1 μM MEK inhibitor
723 PDO325901 (Sigma-Aldrich) and 3 μM GSK-3 inhibitor CHIR9902 (Cayman Chemicals) for 2 days
724 at 37ºC in 5% CO_2 incubator. To reduce evaporation, the area surrounding the wells was filled
725 with DPBS. Embryos were further cultured in a fresh 4-well plates containing, N2B27+2i+LIF
726 media: N2B27 media supplemented with 1 μM MEK inhibitor PDO325901 and 3 μM GSK-3
727 inhibitor and 0.1% LIF for up to 3 days until reaching the blastocyst stage. Each embryo was then
728 transferred to a well of a 96-well plate coated with 0.1% gelatin in DPBS and containing 150 μL of
729 N2B27+2i+LIF media per well. In these conditions, the embryos should attach to the wells allowing
730 the epiblast to form an outgrowth. This plate was then incubated at 37ºC in 5% CO_2 incubator for
731 3 to 7 days until ES-like colonies start to develop from the epiblast outgrowth. Cells were passaged
732 by dissociation with Accutase (Sigma) and seeded in gradual increasing surface area of growth
733 (48-well, 24-well, 12-well plate, T12.5 and T25 flask), until new cell lines were established. At this
734 stage cells were weaned from N2B27+2i+LIF media and then routinely cultured in ES media.

735 **Animals**

736 Mice were maintained and treated in accordance with the Home Office's Animals (Scientific
737 Procedures) Act 1986. All mice were housed on a 10 hr-14 hr light-dark cycle with access to water
738 and food *ad libitum*. Mattings were generally set up in the afternoon. Noon of the day of finding a
739 vaginal plug was designated embryonic day 0.5 (E0.5). Embryo dissection was performed at
740 appropriate timepoints in M2 media (Sigma), using Dumont No.5 forceps (11251-10, FST). No
741 distinction was made between male and female embryos during the analysis.

742 **METHOD DETAILS**

743 **Embryo experiments**

744 Early mouse embryos were isolated at E5.5 (from pregnant CD1 females, purchased from Charles
745 River, UK). Following dissection from the decidua, embryos were cultured overnight in N2B27
746 "poor" media (same formulation as N2B27 media but supplemented with 0.5xB27 supplement and
747 0.5xN2 supplement) with pan-caspase inhibitors (100 μM, Z-VAD-FMK, FMK001, R&D Systems,

748 USA) or equal volume of vehicle (DMSO) as control. On the next morning, embryos were
749 processed for single cell RNA-Seq (scRNA-seq) or functional validation (Δψm analysis and
750 immunohistochemistry for markers of loser cells).
751 For the scRNA-seq and Δψm analysis embryos were dissociated into singe-cells. Briefly, up to 12
752 embryos were dissociated in 600 µL Acccutase (A6964, Sigma, UK) during 12 min at 37ºC,
753 tapping the tube every two minutes. Accutase was then neutralised with equal volume of FCS,
754 cells span down and stained with TMRM, for Δψm analysis, or directly re-suspended in 300 µL
755 DPBS with 1% FCS, for single cell sorting and RNA-seq. Sytox blue (1:1000, S34857,
756 ThermoFisher Scientific, UK), was used as viability staining.

757 **Cell competition assays**

758 Cell competition assays between wild-type and *Bmpr1a*$^{-/-}$, 4n or *Drp1*$^{-/-}$ cells were performed in
759 differentiating conditions. Cells were seeded onto fibronectin-coated plates (1:100, Merck) in
760 DPBS during 1h at 37ºC and grown in N2B27 media - to promote the differentiation of mESCs into
761 a stage resembling the post-implantation epiblast, as cell competition was previously shown to
762 occur in these conditions (Sancho et al., 2013). N2B27 media consisted of 1:1 Dulbecco's modified
763 eagle medium nutrient mixture (DMEM/F12) and Neurobasal supplemented with N2 (1x) and B27
764 (1x) supplements, 2 mM L-glutamine and 0.1 mM β-mercaptoethanol - all from Gibco. Cell
765 competition assays between wild-type and *Mfn2*$^{-/-}$ and between mESCs with different mtDNA
766 content were performed in pluripotency maintenance conditions (ES media).

767 Cells were seeded either separately or mixed for co-cultures at a 50:50 ratio, onto 12 well plates,
768 at a density of 8E04 cells per well, except for assays between wild-type and *Mfn2*$^{-/-}$ mESCs, where
769 3.2E05 cells were seeded per well. The growth of cells was followed daily and compared between
770 separate or co-culture, to control for cell intrinsic growth differences, until the fourth day of culture.
771 Viable cells were counted daily using Vi-CELL XR Analyser (Beckman Coulter, USA), and
772 proportions of each cell type in co-cultures were determined using LSR II Flow Cytometer (BD
773 Bioscience), based on the fluorescent tag of the ubiquitously expressed GFP or TdTomato in one
774 of the cell populations.

775 **Metabolomic Analysis**

776 The metabolic profile was obtained using the Metabolon Platform (Metabolon, Inc). Each sample
777 consisted of 5 biological replicates. For each replicate, 1E07 cells were spun down and snap
778 frozen in liquid nitrogen. Pellets from 5 independent experiments for each condition were analysed
779 by Metabolon Inc by a combination of Ultrahigh Performance Liquid Chromatography-Tandem
780 Mass Spectroscopy (UPLC- MS/MS) and Gas Chromatography-Mass Spectroscopy (GC-MS).
781 Compounds were identified by comparison to library entries of purified standards based on the
782 retention time/index (RI), mass to charge ratio (*m/z)*, and chromatographic data (including MS/MS

783 spectral data) on all molecules present in the library. Samples were normalized to protein content
784 measured by Bradford assay. Statistical analysis was done using Welch's two-sample t-test and
785 statistical significance defined as $p \leq 0.05$.

786 **Analysis of mitochondrial membrane potential (Δψm)**

787 Quantitative analysis of Δψm was performed by flow cytometry. Cells were grown in pluripotency
788 or differentiating conditions, as described above. Cells were dissociated and pelleted to obtain
789 2E05 cells per sample for the staining procedure.

790 For TMRM staining in single cells from early mouse epiblasts, embryos were dissected at E5.5
791 and cultured overnight in the presence or absence of caspase inhibitors. On the following morning,
792 to avoid misleading readings, epiblasts were isolated initially by an enzymatic treatment with of
793 2.5% pancreatin, 0.5% trypsin and 0.5% polyvinylpyrrolidone (PVP40) - all from Sigma-Aldrich- to
794 remove the visceral endoderm (VE). Embryos were treated during 8 min at 4ºC, followed by 2 min
795 at RT. The VE was then pealed with the forceps and the extraembryonic ectoderm removed to
796 isolate the epiblasts. Up to 16 epiblasts were pooled per 600µL of Accutase (Sigma-Aldrich) for
797 dissociation into single cells prior to staining. Reaction was stopped with equal volume of FCS and
798 cells subjected to TMRM staining.

799 Cells were loaded with 10 nM of the Nernstian probe tetramethylrhodamin methyl ester perchlorate
800 (TMRM, Sigma), prepared in N2B27 media. After incubating for 15 min at 37ºC, cells were pelleted
801 again and re-suspended in flow cytometry (FC) buffer (3% FCS in DPBS). Sytox blue (1:1000,
802 Invitrogen, UK) was used as viability staining. Stained cell suspensions were analysed in BD LSRII
803 flow cytometer operated through FACSDiva software (Becton Dickinson Biosciences, UK). For
804 TMRM fluorescence detection the yellow laser was adjusted for excitation at λ=562 nm, capturing
805 the emission light at λ=585 nm for TMRM (Floryk and Houštěk, 1999; Scaduto and Grotyohann,
806 1999). In the case of GFP-labelled cell lines, for GFP fluorescence detection the blue laser was
807 adjusted for excitation at λ=488 nm, capturing the emission light at λ=525 nm. Results were
808 analysed in FlowJo vX10.0.7r2.

809 Qualitative analysis of Δψm was performed by confocal microscopy. Wild-type and *Bmpr1a*$^{-/-}$ cells
810 were grown in fibronectin-coated glass coverslips. At the third day of differentiation, cells were
811 loaded with 200 nM MitoTracker Red probe (Life Technologies), prepared in N2B27 media, for 15
812 min at 37ºC. Cells were then washed with DPBS and fixed with 3.7% formaldehyde for subsequent
813 immunocytochemical staining of total mitochondria mass, with TOMM20 antibody.

814 **Immunofluorescence**

815 Cells were washed with DPBS and fixed with 3.7% formaldehyde (Sigma, UK) in N2B27, for 15
816 min at 37ºC. Permeabilization of the cell membranes was done with 0.4% Triton X-100 in DPBS
817 (DPBS-Tx), at RT with agitation. Blocking step with 5% BSA in DPBS-Tx 0.1% was performed for

818 30 min, at RT with agitation. Mitochondria were labelled with TOMM20 antibody (1:100, Santa
819 Cruz Biotechnologies). Dead cells were labelled with cleaved caspase-3 antibody (1:400, CST)
820 and NANOG antibody was used to mark pluripotent cells (1:100, eBioscience). Secondary
821 antibodies were Alexa Fluor (1:600, Invitrogen). Primary antibody incubation was performed
822 overnight at 4ºC and secondary antibody incubation during 45 min, together with Hoechst to stain
823 nuclei (1:1000, ThermoScientific), at RT and protected from light. In both cases antibodies were
824 diluted in blocking solution. Three 10 min washes with DPBS-Tx 0.1% were performed between
825 each critical step and before mounting with Vectashield medium (Vector Laboratories).

826 Samples were imaged with a Zeiss LSM780 confocal microscope (Zeiss, UK) and processed with
827 Fiji software (Schindelin et al., 2012). Mitochondria stainings were imaged with a 63x/1.4 Oil
828 objective. For samples stained with TOMM20 antibody and MitoTracker Red, Z-stacks were
829 acquired and processed for deconvolution using Huygens software (Scientific Volume Imaging,
830 https://svi.nl/). Samples stained with cleaved caspase-3 were imaged with 20x/0.8 magnification
831 objective. Imaging and deconvolution analysis were performed with the support and advice from
832 Mr. Stephen Rothery from the Facility for Imaging by Light Microscopy (FILM) at Imperial College
833 London.

834 Embryo immunofluorescent staining for p-rpS6, OPA1 and DDIT3 (CHOP) markers was
835 performed as follows. Cultured embryos were fixed in 4% PFA in DPBS containing 0.01% Triton
836 and 0.1% Tween 20 during 20 min at RT. Permeabilization of the membranes was done during
837 10 min in DPBS with 0.5% Triton. Embryos were blocked in 5% BSA in DPBS with 0.25% Triton
838 during 45 min. Incubation with primary antibodies - CHOP (1:500, CST), OPA1 (1:100, BD
839 Biosciences) and p-rpS6 (CST, UK) - was done overnight at 4ºC in 2.5% BSA in DPBS with
840 0.125% Triton. On the following morning, hybridisation with secondary antibodies Alexa Fluor 568
841 and Alexa Fluor 488 (diluted 1:600 in DPBS with 2.5% BSA and 0.125% Triton) was done next
842 during 1h at RT. Hoechst was also added to this mixture to stain nuclei (1:1000). Three 10 min
843 washes with filtered DPBS-Tx 0.1% were performed between each critical step. All steps were
844 done with gentle agitation.

845 Embryos were imaged in embryo dishes (Nunc) in a drop of Vectashield using Zeiss LSM780
846 confocal microscope at 40x magnification.

847 **Western Blotting**

848 Cells were washed in DPBS and lysed with Laemmli lysis buffer (0.05 M Tris- HCl at pH 6.8, 1%
849 SDS, 10% glycerol, 0.1% β-mercaptoethanol in distilled water). Total protein quantification was
850 done using BCA assay (Thermo Scientific, UK) and samples (15µg of protein per lane) were
851 loaded into 12% Bis-Tris protein gels (BioRad). Resolved proteins were transferred into
852 nitrocellulose membranes (GE Healthcare). The following primary antibodies were incubated

853 overnight at 4ºC: rabbit anti-TOMM20 (1:1000, CST-42406), rabbit anti-α-Tubulin (1:1000, CST-
854 2144), mouse anti-mt-CO1 (1:2000, ab14705), rabbit anti-DRP1 (1:1000, CST- 8570), mouse anti-
855 MFN1 (ab57602), mouse anti-MFN2 (ab56889) and mouse anti-Vinculin (1:1000, Sigma V9131).
856 On the following morning, HRP-conjugated secondary antibodies (Santa Cruz) were incubated for
857 1h at RT. Membranes were developed with ECL reagents (Promega) and mounted in cassette
858 for time-time-controlled exposure to film (GE Healthcare).

859 **Bulk RNA-Seq and Single cell RNA-Seq**

860 For bulk RNA Seq in the competitive scenario between cells with different mtDNA, HB(24%) and
861 BG(95%) mESCs were grown separately or in co-culture. On the third day of culture cells were
862 dissociated and subjected to fluorescence activated cell sorting (FACS) to separate the cell
863 populations in co-culture. To control for eventual transcriptional changes due to the FACS process,
864 a mixture of the two separate populations was subjected to the same procedure as the co-cultured
865 samples. Total RNA isolation was then carried out using RNA extraction Kit (RNeasy Mini Kit,
866 Qiagen). PolyA selection/enrichment was the method adopted for library preparation, using the
867 NEB Ultra II RNA Prep Kit. Single end 50bp libraries were sequenced on Illumina Hiseq 2500.
868 Raw basecall files were converted to fastq files using Illumina's bcl2fastq (version 2.1.7). Reads
869 were aligned to mouse genome (mm9) using Tophat2 version 2.0.11 (Kim et al., 2013) with default
870 parameters. Mapped reads that fell on genes were counted using featureCounts from Rsubread
871 package (Liao et al., 2019). Generated count data were then used to identify differentially
872 expressed genes using DESeq2 (Love et al., 2014). Genes with very low read counts were
873 excluded. Finally, Gene Set Enrichment Analysis was performed using GSEA software (Mootha
874 et al., 2003; Subramanian et al., 2005) on pre-ranked list generated by DESeq2.
875 To investigate the nature of cells eliminated by cell competition during early mouse embryogenesis
876 by means of Single Cell RNA-Sequencing (scRNA-seq), early mouse embryos were dissected at
877 E5.5 and cultured overnight in the presence or absence of caspase inhibitors. On the following
878 morning, embryos were dissociated with Accutase and subjected to single-cell sorting into 384-
879 well plate. Total RNA isolation was then carried out using a RNA extraction Kit (RNeasy Mini Kit,
880 Qiagen). scRNA-seq was performed using the Smart-Seq2 illumina method. PolyA
881 selection/enrichment with Ultra II Kit (NEB) was the method adopted for library preparation.

882 **Data processing, quality control and normalization**

883 We performed transcript quantification in our scRNA-seq data by running Salmon v0.8.2 (Patro et
884 al., 2017) in the quasi-mapping-based mode. First, a transcriptome index was created from the
885 mouse reference (version GRCm38.p4) and ERCC spike-in sequences. Then, the quantification
886 step was carried out with the "quant" function, correcting for the sequence-specific biases ("--
887 seqBias" flag) and the fragment-level GC biases ("--gcBias" flag). Finally, the transcript level

888 abundances were aggregated to gene level counts. On the resulting raw count matrix including
889 1,495 cells, we apply a quality control to exclude poor quality cells from downstream analyses.
890 For the quality control we used the following criteria: we identified the cells that have a log10 total
891 number of reads equal to or greater than 4, a fraction of mapped reads equal to or greater than
892 0.8, a number of genes with expression level above 10 reads per million equal to or greater than
893 3000 and a fraction of reads mapped to endogenous genes equal to or greater than 0.5. This
894 resulted in the selection of 723 cells, which were kept for downstream analyses. Transcripts per
895 million (TPM) normalization (as estimated by Salmon) was used.

896 **Identification of highly variable genes and dimensionality reduction**

897 To identify highly variable genes (HVG), first we fitted a mean-total variance trend using the R
898 function "trendVar" and then the variance was decomposed into biological and technical
899 components with the R function "decomposeVar"; both functions are included in the package
900 "scran" (version 1.6.9 (Lun et al., 2016)).
901 We considered HVGs those that have a biological component that is significantly greater than zero
902 at a false discovery rate (Benjamini-Hochberg method) of 0.05. Then, we applied further filtering
903 steps by keeping only genes that have an average expression greater to or equal than 10 TPM
904 and are significantly correlated with one another (function "correlatePairs" in "scran" package,
905 FDR<0.05). This yielded 1921 genes, which were used to calculate a distance matrix between
906 cells defined as $\sqrt{(1-\rho)/2}$, where ρ is the Spearman's correlation coefficient between cells. A
907 2D representation of the data was obtained with UMAP package (version 0.2.0.0 https://cran.r-
908 project.org/web/packages/umap/index.html) using the distance matrix as input.

909 **Cell clustering**

910 To classify cells into different clusters, we ran hierarchical clustering on the distance matrix (see
911 above; "hclust" function in R with ward.D2 aggregation method) followed by the dynamic hybrid
912 cut algorithm ("cutreeDynamic" function in R package "dynamicTreeCut" (https://CRAN.R-
913 project.org/package=dynamicTreeCut) version 1.63.1, with the hybrid method, a minimum cluster
914 size of 35 cells and a "deepSplit" parameter equal to 0), which identified five clusters. Cells from
915 different batches were well mixed across these five clusters (see Figure S1), suggesting that the
916 batch effect was negligible.

917 **Identification of a single-cell trajectory in the epiblast**

918 We calculated a diffusion map ("DiffusionMap" function in the R package "destiny" version 2.6.2
919 (Angerer et al., 2016) on the distance defined above on the epiblast cells from CI-treated embryos.
920 The pseudotime coordinate was computed with the "DPT" function with the root cell in the winner
921 epiblast cluster (identified by the function "tips" in the "destiny" package). Such pseudotime

922 coordinate can be interpreted as a “losing score” for all the epiblast cells from the CI-treated
923 embryos.
924 We estimated the losing scores of the epiblast cells from DMSO-treated embryos by projecting
925 such data onto the diffusion map previously calculated (function “dm_predict” in the destiny
926 package). Finally, for each of the projected cells, we assigned the losing score as the average of
927 the losing scores of the 10 closest neighbours in the original diffusion map (detected with the
928 function “projection-dist” in the destiny package).

929 **Differential gene expression analysis along the trajectory**

930 To identify the genes that are differentially expressed along the trajectory, first we kept only genes
931 that have more than 15 TPM in more than 10 cells (this list of genes is provided in Supplementary
932 Table 4); then, we obtained the log-transformed expression levels of these genes (adding 1 as a
933 pseudo-count to avoid infinities) as a function of the losing score and we fitted a generalized
934 additive model to them (R function “gam” from “GAM” package version 1.16.). We used the
935 ANOVA test for parametric effect provided by the gam function to estimate a p-value for each
936 tested gene. This yielded a list of 5,311 differentially expressed genes (FDR < 0.01).
937 Next, we looked for groups of differentially expressed genes that share similar expression patterns
938 along the trajectory. To this aim, similarly to what we did when clustering cells, we calculated a
939 correlation-based distance matrix between genes, defined as $\sqrt{(1-\rho)/2}$, where ρ is the
940 Spearman’s correlation coefficient between genes. Hierarchical clustering was then applied to this
941 matrix (hclust function in R, with ward.D2 method) followed by the dynamic hybrid cut algorithm
942 (dynamicTreeCut package) to define clusters (“cutreeDynamic” function in R with the hybrid
943 method and a minimum cluster size of 100 genes and a deepSplit parameter equal to 0). This
944 resulted in the definition of four clusters, three of genes that decrease along the trajectory (merged
945 together for the GO enrichment and the IPA analysis) and one of increasing genes (Figure S2D).
946 IPA (QIAGEN Inc., https://www.qiagenbio- informatics.com/products/ingenuity-pathway-analysis),
947 was run on all genes differentially expressed (FDR < 0.01) along the trajectory from winner to loser
948 cells (see Figures 2A-D and Figures 3A-C), using all the tested genes as a background (see
949 Supplementary Table 4). This software generated networks, canonical pathways and functional
950 analysis. The list of decreasing/increasing genes is provided in Supplementary Tables 1 and 2.

951 **Analysis of Mitochondrial DNA heteroplasmy**

952 We used STAR (version 2.7 (Dobin et al., 2013)) to align the transcriptome of the epiblast cells
953 from CI-treated embryos (274) to the mouse reference genome (mm10). Only reads that uniquely
954 mapped to the mitochondrial DNA (mtDNA) were considered. From these, we obtained allele
955 counts at each mtDNA position with a Phred Quality Score greater than 33 using the samtools
956 mpileup function.

957 Next, we applied filters to remove cells and mtDNA positions with a low coverage. First, we
958 removed cells with fewer than 2,000 mtDNA positions covered by more than 50 reads. Second,
959 we removed positions having less than 50 reads in more than 50% of cells in each of the three
960 epiblast clusters (winner, intermediate and loser). These two filters resulted in 259 cells and 5,192
961 mtDNA positions being considered for further analyses.
962 Starting from these cells and positions, we applied an additional filter to keep only positions with
963 a sufficiently high level of heteroplasmy. To this aim, for each position with more than 50 reads in
964 a cell, we estimated the heteroplasmy as:

965 $$H = 1 - f_{max}$$

966 where f_{max} is the frequency of the most common allele. We kept only positions with H>0.01 in at
967 least 10 cells.
968 Finally, using generalized additive models (see above), we identified the positions whose
969 heteroplasmy H changes as a function of the cells' losing score in a statistically significant way.
970 We found a total of eleven significant positions (FDR < 0.001), six of them in the *mt-Rnr1* gene
971 and five in the *mt-Rnr2* gene. All of these positions have a higher level of heteroplasmy in loser
972 cells (see Figure 6B-G and Figure S5F-K). The results remain substantially unaltered if the
973 Spearman's rank correlation test (in alternative to the generalized additive models) is used.
974 For the barplot shown in Figure 6H and the correlation heatmaps in Figure 6I and S5L, we took
975 into account only cells that covered with more than 50 reads all the significant positions in the *mt-*
976 *Rnr1* gene (215 cells, Figures 6H and 6I) or in both the *mt-Rnr1* and *mt-Rnr2* genes (214 cells,
977 Figure S5L).
978 As a negative control, we repeated the analysis described above using the ERCC spike-ins added
979 to each cell. As expected, none of the positions was statistically significant, which suggested that
980 our procedure is robust against sequence errors introduced during PCR amplification.

981 **Common features of scRNA-seq and bulk RNA-seq datasets**

982 Differential expression analysis between the co-cultured winner HB(24%) and loser cell line
983 BG(95%) was performed using the package EdgeR version 3.20.9 (Robinson et al., 2010).
984 Batches were specified in the argument of the function model.matrix. We fitted a quasi-likelihood
985 negative binomial generalized log-linear model (with the function glmQLFit) to the genes that were
986 filtered by the function filterByExpr (with default parameter). These genes were used as
987 background for the gene enrichment analysis.
988 We set a FDR of 0.001 as a threshold for significance. The enrichment analysis for both the
989 scRNA-seq and bulk RNA-seq datasets were performed using the tool g:Profiler (Reimand et al.,
990 2011). The list of up-regulated, down-regulated and background genes related to the DE analysis
991 for the bulk RNA-seq dataset are provided in the Supplementary Tables 5, 6 and 7.

992 **Quantification and Statistical Analysis**

993 Flow cytometry data was analysed with FlowJo Software.

994 Western blot quantification was performed using Image Studio Lite (LI-COR). Protein expression
995 levels were normalised to loading controls vinculin or α-tubulin.

996 The quantification of the DDIT3 and OPA1 expression in embryos was done by two distinct
997 methods. DDIT3 expression was quantified by counting the number of epiblast cells with positive
998 staining in the embryos of each group. The expression of OPA1 was quantified on Fiji software as
999 the mean fluorescence across a 10 pixel width line drawn on the basal cytoplasm of each cell with
1000 high or low p-rpS6 fluorescence intensity, as specified in (Bowling *et al.*, 2018). A min of 8 cells
1001 were quantified per condition (high vs low mTOR activity) in each embryo. Six embryos treated
1002 with CI were analysed. Mean grey values of OPA1 fluorescence for each epiblast cell are pooled
1003 on the same graph.

1004 The statistical analysis of the results was performed using GraphPad Prism v8 Software
1005 (GraphPad Software, United States of America). Data was tested for normality using Shapiro-Wilk
1006 normality test. Parametric or non-parametric statistical tests were applied accordingly. Details
1007 about the test used in each of the experiments are specified in figure legends. Statistical
1008 significance was considered with a confidence interval of 0.05%. n.s., non-significant; * $p<0.05$; **
1009 $p<0.01$;*** $p<0.001$.

1010 **Data and Code Availability**

1011 Data were analysed with standard programs and packages, as detailed above. Code is available
1012 on request. Raw as well as processed data are available through ArrayExpress, accession
1013 numbers E-MTAB-8640, for scRNA-seq data, and E-MTAB-8692, for bulk RNA-seq data.

1014 # References

1015 Allio, R., Donega, S., Galtier, N., and Nabholz, B. (2017). Large Variation in the Ratio of
1016 Mitochondrial to Nuclear Mutation Rate across Animals: Implications for Genetic Diversity and
1017 the Use of Mitochondrial DNA as a Molecular Marker. Mol Biol Evol *34*, 2762-2772.
1018 Angerer, P., Haghverdi, L., Buttner, M., Theis, F.J., Marr, C., and Buettner, F. (2016). destiny:
1019 diffusion maps for large-scale single-cell data in R. Bioinformatics *32*, 1241-1243.
1020 Bowling, S., Di Gregorio, A., Sancho, M., Pozzi, S., Aarts, M., Signore, M., M, D.S., Barbera,
1021 J.P.M., Gil, J., and Rodriguez, T.A. (2018). P53 and mTOR signalling determine fitness selection
1022 through cell competition during early mouse embryonic development. Nat Commun *9*, 1763.
1023 Bowling, S., Lawlor, K., and Rodriguez, T.A. (2019). Cell competition: the winners and losers of
1024 fitness selection. Development *146*.
1025 Burgstaller, J.P., Johnston, I.G., Jones, N.S., Albrechtova, J., Kolbe, T., Vogl, C., Futschik, A.,
1026 Mayrhofer, C., Klein, D., Sabitzer, S.*, et al.* (2014). MtDNA segregation in heteroplasmic tissues
1027 is common in vivo and modulated by haplotype differences and developmental stage. Cell Rep
1028 *7*, 2031-2041.
1029 Burgstaller, J.P., Johnston, I.G., and Poulton, J. (2015). Mitochondrial DNA disease and
1030 developmental implications for reproductive strategies. Mol Hum Reprod *21*, 11-22.
1031 Burr, S.P., Pezet, M., and Chinnery, P.F. (2018). Mitochondrial DNA Heteroplasmy and Purifying
1032 Selection in the Mammalian Female Germ Line. Dev Growth Differ *60*, 21-32.
1033 Chen, H., Detmer, S.A., Ewald, A.J., Griffin, E.E., Fraser, S.E., and Chan, D.C. (2003).
1034 Mitofusins Mfn1 and Mfn2 coordinately regulate mitochondrial fusion and are essential for
1035 embryonic development. J Cell Biol *160*, 189-200.
1036 Chinnery, P.F., and Hudson, G. (2013). Mitochondrial genetics. Br Med Bull *106*, 135-159.
1037 Claveria, C., Giovinazzo, G., Sierra, R., and Torres, M. (2013). Myc-driven endogenous cell
1038 competition in the early mammalian embryo. Nature *500*, 39-44.
1039 Czechanski, A., Byers, C., Greenstein, I., Schrode, N., Donahue, L.R., Hadjantonakis, A.K., and
1040 Reinholdt, L.G. (2014). Derivation and characterization of mouse embryonic stem cells from
1041 permissive and nonpermissive strains. Nat Protoc *9*, 559-574.
1042 Di-Gregorio, A., Sancho, M., Stuckey, D.W., Crompton, L.A., Godwin, J., Mishina, Y., and
1043 Rodriguez, T.A. (2007). BMP signalling inhibits premature neural differentiation in the mouse
1044 embryo. Development *134*, 3359-3369.
1045 Diaz-Diaz, C., Fernandez de Manuel, L., Jimenez-Carretero, D., Montoya, M.C., Claveria, C.,
1046 and Torres, M. (2017). Pluripotency Surveillance by Myc-Driven Competitive Elimination of
1047 Differentiating Cells. Dev Cell *42*, 585-599 e584.
1048 Diaz-Diaz, C., and Torres, M. (2019). Insights into the quantitative and dynamic aspects of Cell
1049 Competition. Curr Opin Cell Biol *60*, 68-74.
1050 Dobin, A., Davis, C.A., Schlesinger, F., Drenkow, J., Zaleski, C., Jha, S., Batut, P., Chaisson, M.,
1051 and Gingeras, T.R. (2013). STAR: ultrafast universal RNA-seq aligner. Bioinformatics *29*, 15-21.
1052 Ellis, S.J., Gomez, N.C., Levorse, J., Mertz, A.F., Ge, Y., and Fuchs, E. (2019). Distinct modes
1053 of cell competition shape mammalian tissue morphogenesis. Nature *569*, 497-502.
1054 Fan, W., Waymire, K.G., Narula, N., Li, P., Rocher, C., Coskun, P.E., Vannan, M.A., Narula, J.,
1055 Macgregor, G.R., and Wallace, D.C. (2008). A mouse model of mitochondrial disease reveals
1056 germline selection against severe mtDNA mutations. Science *319*, 958-962.
1057 Fischer, M. (2017). Census and evaluation of p53 target genes. Oncogene *36*, 3943-3956.
1058 Floros, V.I., Pyle, A., Dietmann, S., Wei, W., Tang, W.C.W., Irie, N., Payne, B., Capalbo, A.,
1059 Noli, L., Coxhead, J.*, et al.* (2018). Segregation of mitochondrial DNA heteroplasmy through a
1060 developmental genetic bottleneck in human embryos. Nat Cell Biol *20*, 144-151.
1061 Freyer, C., Cree, L.M., Mourier, A., Stewart, J.B., Koolmeister, C., Milenkovic, D., Wai, T.,
1062 Floros, V.I., Hagstrom, E., Chatzidaki, E.E.*, et al.* (2012). Variation in germline mtDNA
1063 heteroplasmy is determined prenatally but modified during subsequent transmission. Nat Genet
1064 *44*, 1282-1285.
1065 Gorman, G.S., Chinnery, P.F., DiMauro, S., Hirano, M., Koga, Y., McFarland, R., Suomalainen,
1066 A., Thorburn, D.R., Zeviani, M., and Turnbull, D.M. (2016). Mitochondrial diseases. Nat Rev Dis
1067 Primers *2*, 16080.

1068 Haghverdi, L., Buttner, M., Wolf, F.A., Buettner, F., and Theis, F.J. (2016). Diffusion pseudotime
1069 robustly reconstructs lineage branching. Nature methods *13*, 845-848.
1070 Hashimoto, M., and Sasaki, H. (2019). Epiblast Formation by TEAD-YAP-Dependent Expression
1071 of Pluripotency Factors and Competitive Elimination of Unspecified Cells. Dev Cell *50*, 139-154
1072 e135.
1073 Johnston, I.G., Burgstaller, J.P., Havlicek, V., Kolbe, T., Rulicke, T., Brem, G., Poulton, J., and
1074 Jones, N.S. (2015). Stochastic modelling, Bayesian inference, and new in vivo measurements
1075 elucidate the debated mtDNA bottleneck mechanism. Elife *4*, e07464.
1076 Kauppila, J.H.K., Baines, H.L., Bratic, A., Simard, M.L., Freyer, C., Mourier, A., Stamp, C.,
1077 Filograna, R., Larsson, N.G., Greaves, L.C.*, et al.* (2016). A Phenotype-Driven Approach to
1078 Generate Mouse Models with Pathogenic mtDNA Mutations Causing Mitochondrial Disease. Cell
1079 Rep *16*, 2980-2990.
1080 Khrapko, K., Coller, H.A., Andre, P.C., Li, X.C., Hanekamp, J.S., and Thilly, W.G. (1997).
1081 Mitochondrial mutational spectra in human cells and tissues. Proc Natl Acad Sci U S A *94*,
1082 13798-13803.
1083 Kim, D., Pertea, G., Trapnell, C., Pimentel, H., Kelley, R., and Salzberg, S.L. (2013). TopHat2:
1084 accurate alignment of transcriptomes in the presence of insertions, deletions and gene fusions.
1085 Genome Biol *14*, R36.
1086 Kojima, Y., Kaufman-Francis, K., Studdert, J.B., Steiner, K.A., Power, M.D., Loebel, D.A., Jones,
1087 V., Hor, A., de Alencastro, G., Logan, G.J.*, et al.* (2014). The transcriptional and functional
1088 properties of mouse epiblast stem cells resemble the anterior primitive streak. Cell Stem Cell *14*,
1089 107-120.
1090 Kon, S., Ishibashi, K., Katoh, H., Kitamoto, S., Shirai, T., Tanaka, S., Kajita, M., Ishikawa, S.,
1091 Yamauchi, H., Yako, Y.*, et al.* (2017). Cell competition with normal epithelial cells promotes
1092 apical extrusion of transformed cells through metabolic changes. Nat Cell Biol *19*, 530-541.
1093 Kramer, A., Green, J., Pollard, J., Jr., and Tugendreich, S. (2014). Causal analysis approaches
1094 in Ingenuity Pathway Analysis. Bioinformatics *30*, 523-530.
1095 Kucinski, I., Dinan, M., Kolahgar, G., and Piddini, E. (2017). Chronic activation of JNK JAK/STAT
1096 and oxidative stress signalling causes the loser cell status. Nat Commun *8*, 136.
1097 Latorre-Pellicer, A., Lechuga-Vieco, A.V., Johnston, I.G., Hamalainen, R.H., Pellico, J., Justo-
1098 Mendez, R., Fernandez-Toro, J.M., Claveria, C., Guaras, A., Sierra, R.*, et al.* (2019). Regulation
1099 of Mother-to-Offspring Transmission of mtDNA Heteroplasmy. Cell Metab.
1100 Lee, H.S., Ma, H., Juanes, R.C., Tachibana, M., Sparman, M., Woodward, J., Ramsey, C., Xu,
1101 J., Kang, E.J., Amato, P.*, et al.* (2012). Rapid mitochondrial DNA segregation in primate
1102 preimplantation embryos precedes somatic and germline bottleneck. Cell Rep *1*, 506-515.
1103 Liao, Y., Smyth, G.K., and Shi, W. (2019). The R package Rsubread is easier, faster, cheaper
1104 and better for alignment and quantification of RNA sequencing reads. Nucleic Acids Res *47*,
1105 e47.
1106 Lima, A., Burgstaller, J., Sanchez-Nieto, J.M., and Rodriguez, T.A. (2018). The Mitochondria and
1107 the Regulation of Cell Fitness During Early Mammalian Development. Curr Top Dev Biol *128*,
1108 339-363.
1109 Love, M.I., Huber, W., and Anders, S. (2014). Moderated estimation of fold change and
1110 dispersion for RNA-seq data with DESeq2. Genome Biol *15*, 550.
1111 Ludwig, L.S., Lareau, C.A., Ulirsch, J.C., Christian, E., Muus, C., Li, L.H., Pelka, K., Ge, W.,
1112 Oren, Y., Brack, A.*, et al.* (2019). Lineage Tracing in Humans Enabled by Mitochondrial
1113 Mutations and Single-Cell Genomics. Cell *176*, 1325-1339 e1322.
1114 Lun, A.T., McCarthy, D.J., and Marioni, J.C. (2016). A step-by-step workflow for low-level
1115 analysis of single-cell RNA-seq data with Bioconductor. F1000Res *5*, 2122.
1116 Madan, E., Gogna, R., and Moreno, E. (2018). Cell competition in development: information from
1117 flies and vertebrates. Curr Opin Cell Biol *55*, 150-157.
1118 Melber, A., and Haynes, C.M. (2018). UPR(mt) regulation and output: a stress response
1119 mediated by mitochondrial-nuclear communication. Cell Res *28*, 281-295.
1120 Mootha, V.K., Lindgren, C.M., Eriksson, K.F., Subramanian, A., Sihag, S., Lehar, J., Puigserver,
1121 P., Carlsson, E., Ridderstrale, M., Laurila, E.*, et al.* (2003). PGC-1alpha-responsive genes

1122 involved in oxidative phosphorylation are coordinately downregulated in human diabetes. Nat
1123 Genet *34*, 267-273.
1124 Morata, G., and Ripoll, P. (1975). Minutes: mutants of drosophila autonomously affecting cell
1125 division rate. Dev Biol *42*, 211-221.
1126 Mouchiroud, L., Houtkooper, R.H., Moullan, N., Katsyuba, E., Ryu, D., Canto, C., Mottis, A., Jo,
1127 Y.S., Viswanathan, M., Schoonjans, K.*, et al.* (2013). The NAD(+)/Sirtuin Pathway Modulates
1128 Longevity through Activation of Mitochondrial UPR and FOXO Signaling. Cell *154*, 430-441.
1129 Munch, C. (2018). The different axes of the mammalian mitochondrial unfolded protein
1130 response. BMC Biol *16*, 81.
1131 Nargund, A.M., Pellegrino, M.W., Fiorese, C.J., Baker, B.M., and Haynes, C.M. (2012).
1132 Mitochondrial import efficiency of ATFS-1 regulates mitochondrial UPR activation. Science *337*,
1133 587-590.
1134 Patro, R., Duggal, G., Love, M.I., Irizarry, R.A., and Kingsford, C. (2017). Salmon provides fast
1135 and bias-aware quantification of transcript expression. Nat Methods *14*, 417-419.
1136 Prudent, J., and McBride, H.M. (2017). The mitochondria-endoplasmic reticulum contact sites: a
1137 signalling platform for cell death. Curr Opin Cell Biol *47*, 52-63.
1138 Quiros, P.M., Mottis, A., and Auwerx, J. (2016). Mitonuclear communication in homeostasis and
1139 stress. Nat Rev Mol Cell Biol *17*, 213-226.
1140 Quiros, P.M., Prado, M.A., Zamboni, N., D'Amico, D., Williams, R.W., Finley, D., Gygi, S.P., and
1141 Auwerx, J. (2017). Multi-omics analysis identifies ATF4 as a key regulator of the mitochondrial
1142 stress response in mammals. J Cell Biol *216*, 2027-2045.
1143 Rajasimha, H.K., Chinnery, P.F., and Samuels, D.C. (2008). Selection against pathogenic
1144 mtDNA mutations in a stem cell population leads to the loss of the 3243A-->G mutation in blood.
1145 Am J Hum Genet *82*, 333-343.
1146 Ran, F.A., Hsu, P.D., Wright, J., Agarwala, V., Scott, D.A., and Zhang, F. (2013). Genome
1147 engineering using the CRISPR-Cas9 system. Nat Protoc *8*, 2281-2308.
1148 Reimand, J., Arak, T., and Vilo, J. (2011). g:Profiler--a web server for functional interpretation of
1149 gene lists (2011 update). Nucleic Acids Res *39*, W307-315.
1150 Robinson, M.D., McCarthy, D.J., and Smyth, G.K. (2010). edgeR: a Bioconductor package for
1151 differential expression analysis of digital gene expression data. Bioinformatics *26*, 139-140.
1152 Sancho, M., Di-Gregorio, A., George, N., Pozzi, S., Sanchez, J.M., Pernaute, B., and Rodriguez,
1153 T.A. (2013). Competitive interactions eliminate unfit embryonic stem cells at the onset of
1154 differentiation. Dev Cell *26*, 19-30.
1155 Saveljeva, S., Cleary, P., Mnich, K., Ayo, A., Pakos-Zebrucka, K., Patterson, J.B., Logue, S.E.,
1156 and Samali, A. (2016). Endoplasmic reticulum stress-mediated induction of SESTRIN 2
1157 potentiates cell survival. Oncotarget *7*, 12254-12266.
1158 Schindelin, J., Arganda-Carreras, I., Frise, E., Kaynig, V., Longair, M., Pietzsch, T., Preibisch,
1159 S., Rueden, C., Saalfeld, S., Schmid, B.*, et al.* (2012). Fiji: an open-source platform for
1160 biological-image analysis. Nat Methods *9*, 676-682.
1161 Sharpley, M.S., Marciniak, C., Eckel-Mahan, K., McManus, M., Crimi, M., Waymire, K., Lin, C.S.,
1162 Masubuchi, S., Friend, N., Koike, M.*, et al.* (2012). Heteroplasmy of mouse mtDNA is genetically
1163 unstable and results in altered behavior and cognition. Cell *151*, 333-343.
1164 Smirnova, E., Griparic, L., Shurland, D.L., and van der Bliek, A.M. (2001). Dynamin-related
1165 protein Drp1 is required for mitochondrial division in mammalian cells. Mol Biol Cell *12*, 2245-
1166 2256.
1167 Snow, M.H. (1977). Gastrulation in the mouse: Growth and regionalization of the epiblast.
1168 Development *42*, 293-303.
1169 Stewart, J.B., Freyer, C., Elson, J.L., Wredenberg, A., Cansu, Z., Trifunovic, A., and Larsson,
1170 N.G. (2008). Strong purifying selection in transmission of mammalian mitochondrial DNA. PLoS
1171 Biol *6*, e10.
1172 Stower, M.J., and Srinivas, S. (2018). The Head's Tale: Anterior-Posterior Axis Formation in the
1173 Mouse Embryo. Curr Top Dev Biol *128*, 365-390.
1174 Subramanian, A., Tamayo, P., Mootha, V.K., Mukherjee, S., Ebert, B.L., Gillette, M.A.,
1175 Paulovich, A., Pomeroy, S.L., Golub, T.R., Lander, E.S.*, et al.* (2005). Gene set enrichment

1176 analysis: a knowledge-based approach for interpreting genome-wide expression profiles. Proc
1177 Natl Acad Sci U S A *102*, 15545-15550.
1178 Topf, U., Wrobel, L., and Chacinska, A. (2016). Chatty Mitochondria: Keeping Balance in
1179 Cellular Protein Homeostasis. Trends Cell Biol *26*, 577-586.
1180 Yun, J., and Finkel, T. (2014). Mitohormesis. Cell Metab *19*, 757-766.
1181 Zhang, H., Burr, S.P., and Chinnery, P.F. (2018). The mitochondrial DNA genetic bottleneck:
1182 inheritance and beyond. Essays Biochem *62*, 225-234.
1183 Zhao, Q., Wang, J., Levichkin, I.V., Stasinopoulos, S., Ryan, M.T., and Hoogenraad, N.J. (2002).
1184 A mitochondrial specific stress response in mammalian cells. EMBO J *21*, 4411-4419.
1185 Zhou, W., Choi, M., Margineantu, D., Margaretha, L., Hesson, J., Cavanaugh, C., Blau, C.A.,
1186 Horwitz, M.S., Hockenbery, D., Ware, C.*, et al.* (2012). HIF1alpha induced switch from bivalent
1187 to exclusively glycolytic metabolism during ESC-to-EpiSC/hESC transition. EMBO J *31*, 2103-
1188 2116.
1189

Graphical Abstract

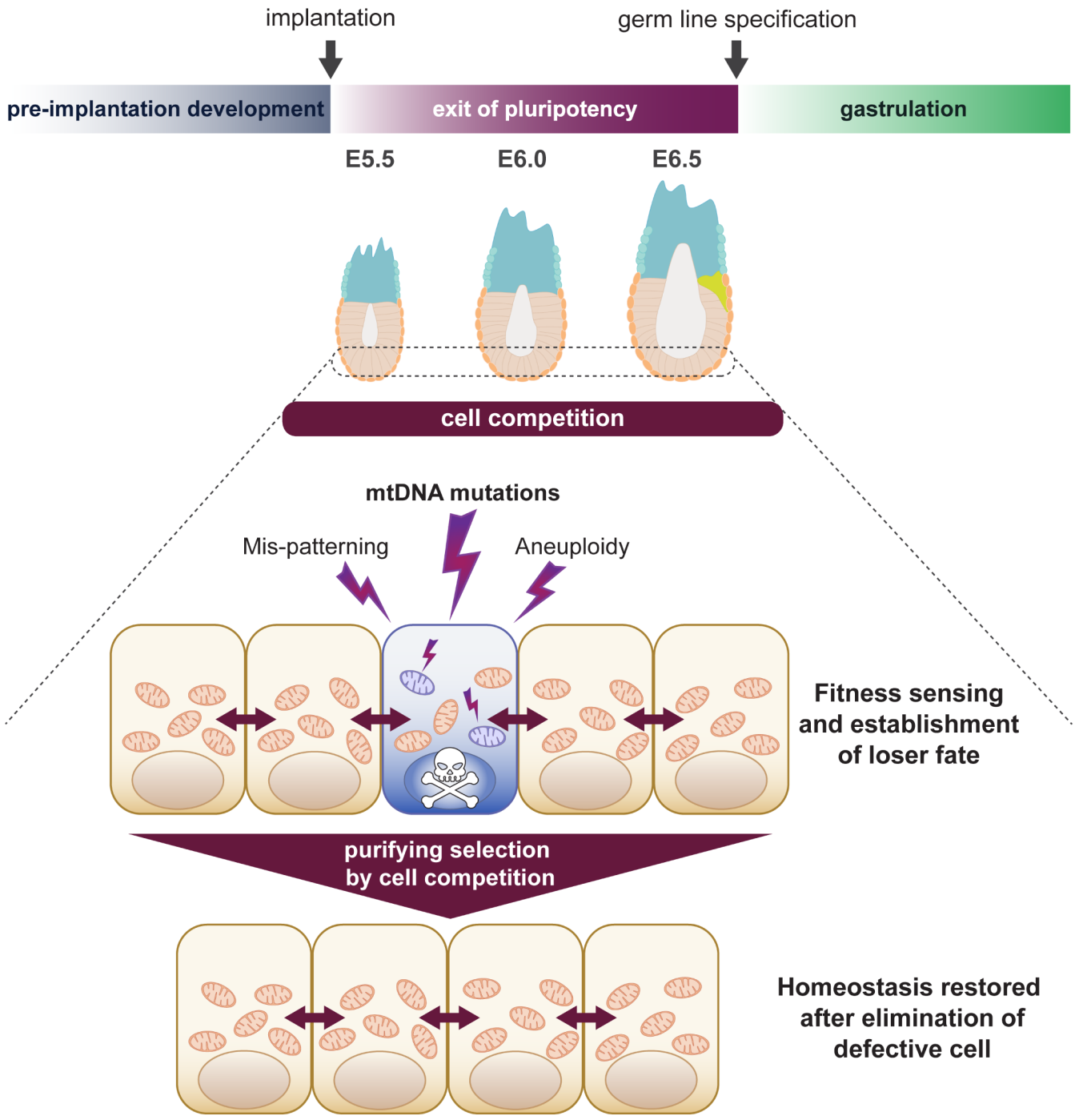

Fig. 1

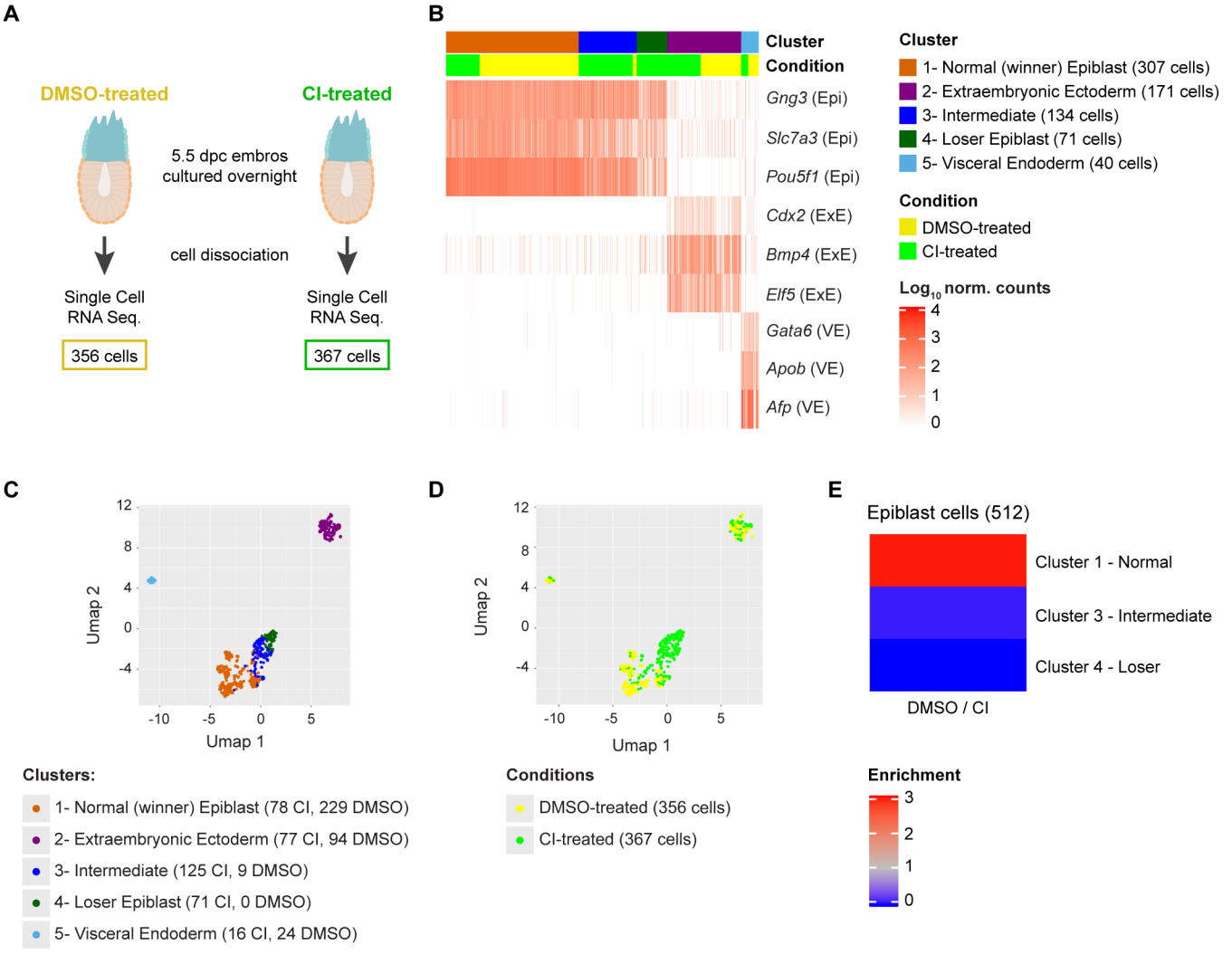
A
DMSO-treated
CI-treated
5.5 dpc embros cultured overnight
cell dissociation
Single Cell RNA Seq.
356 cells
Single Cell RNA Seq.
367 cells
B
Cluster
Condition
Gng3 (Epi)
Slc7a3 (Epi)
Pou5f1 (Epi)
Cdx2 (ExE)
Bmp4 (ExE)
Elf5 (ExE)
Gata6 (VE)
Apob (VE)
Afp (VE)
Cluster
1- Normal (winner) Epiblast (307 cells)
2- Extraembryonic Ectoderm (171 cells)
3- Intermediate (134 cells)
4- Loser Epiblast (71 cells)
5- Visceral Endoderm (40 cells)
Condition
DMSO-treated
CI-treated
Log10 norm. counts
4
3
2
1
0
C
Umap 2
Umap 1
Clusters:
1- Normal (winner) Epiblast (78 CI, 229 DMSO)
2- Extraembryonic Ectoderm (77 CI, 94 DMSO)
3- Intermediate (125 CI, 9 DMSO)
4- Loser Epiblast (71 CI, 0 DMSO)
5- Visceral Endoderm (16 CI, 24 DMSO)
D
Umap 2
Umap 1
Conditions
DMSO-treated (356 cells)
CI-treated (367 cells)
E
Epiblast cells (512)
Cluster 1 - Normal
Cluster 3 - Intermediate
Cluster 4 - Loser
DMSO / CI
Enrichment
3
2
1
0

Fig. 2

A

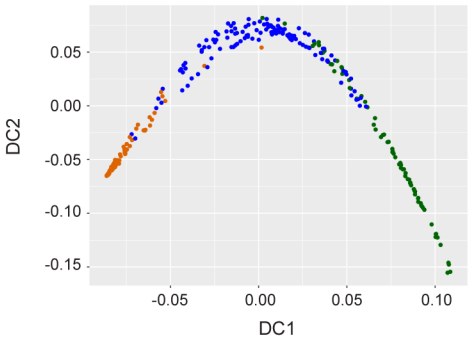

Clusters:

- 1- Normal (winner) Epiblast
- 3- Intermediate
- 4- Loser Epiblast

B

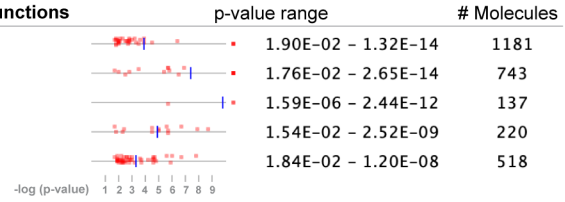

C

Upstream Regulator	Molecule Type	Experimental FDR	p-value of overlap
RICTOR	other	9.3E-04	3.5E-33
TLE3	other	-	1.2E-18
MYC	transcription regulator	-	1.1E-16
MYCN	transcription regulator	2.3E-10	5.6E-16
TP53	transcription regulator	-	3.8E-13
IGF1R	transmembrane receptor	-	1.1E-12
STK11	kinase	-	4.0E-12
NFE2L2	transcription regulator	1.6E-10	7.8E-12
INSR	kinase	-	1.2E-11
LONP1	peptidase	1.1E-06	2.7E-11

D

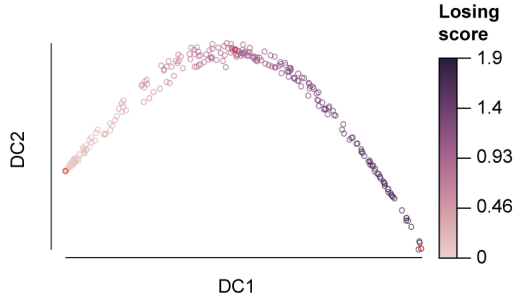

E

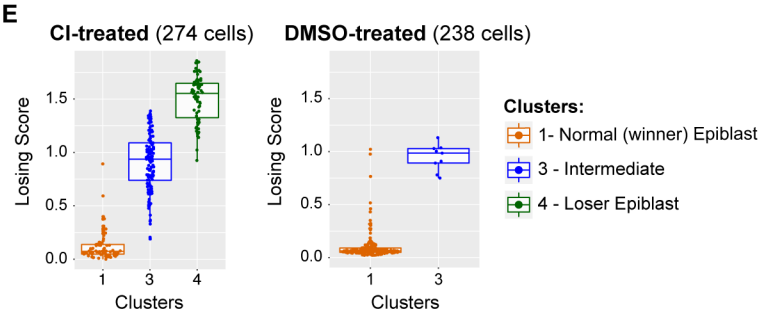

F

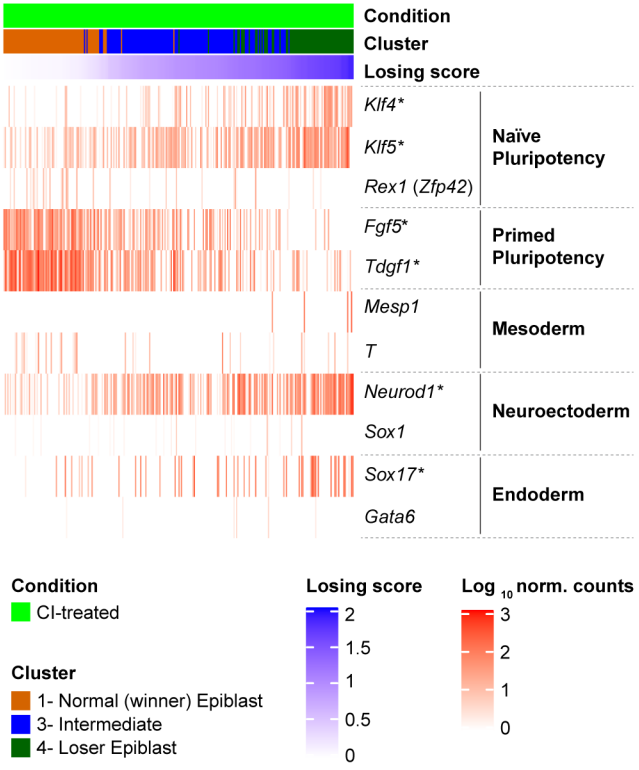

G

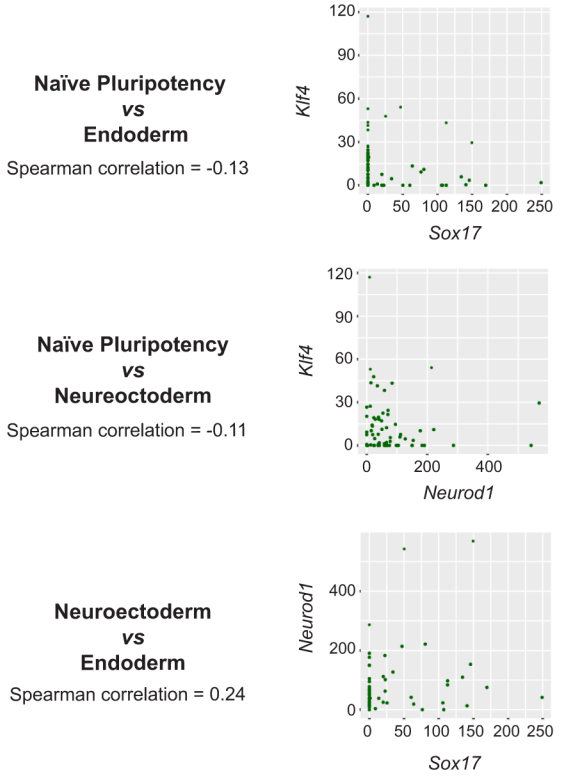

Fig. 3

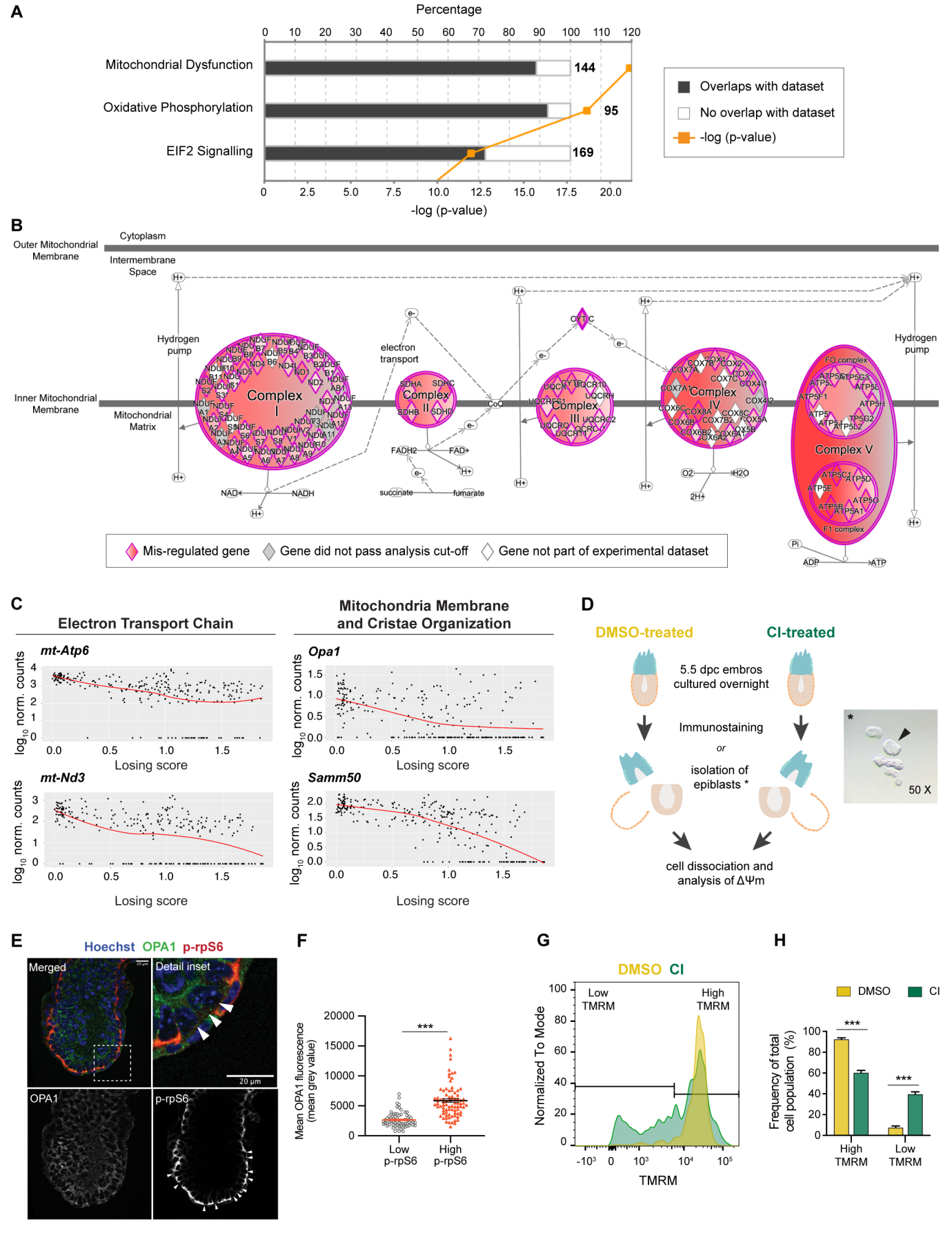
A
Percentage
Mitochondrial Dysfunction
Oxidative Phosphorylation
EIF2 Signalling
144
95
169
-log (p-value)
Overlaps with dataset
No overlap with dataset
-log (p-value)
B
Cytoplasm
Outer Mitochondrial Membrane
Intermembrane Space
Inner Mitochondrial Membrane
Mitochondrial Matrix
Hydrogen pump
electron transport
Complex I
Complex II
Complex III
Complex IV
Complex V
Mis-regulated gene
Gene did not pass analysis cut-off
Gene not part of experimental dataset
C
Electron Transport Chain
Mitochondria Membrane and Cristae Organization
mt-Atp6
mt-Nd3
Opa1
Samm50
log10 norm. counts
Losing score
D
DMSO-treated
CI-treated
5.5 dpc embros cultured overnight
Immunostaining
or
isolation of epiblasts *
cell dissociation and analysis of ΔΨm
50 X
E
Hoechst OPA1 p-rpS6
Merged
Detail inset
OPA1
p-rpS6
20 µm
F
Mean OPA1 fluorescence (mean grey value)
Low p-rpS6
High p-rpS6
***
G
DMSO CI
Low TMRM
High TMRM
Normalized To Mode
TMRM
H
DMSO
CI
Frequency of total cell population (%)
High TMRM
Low TMRM
***

Fig. 4

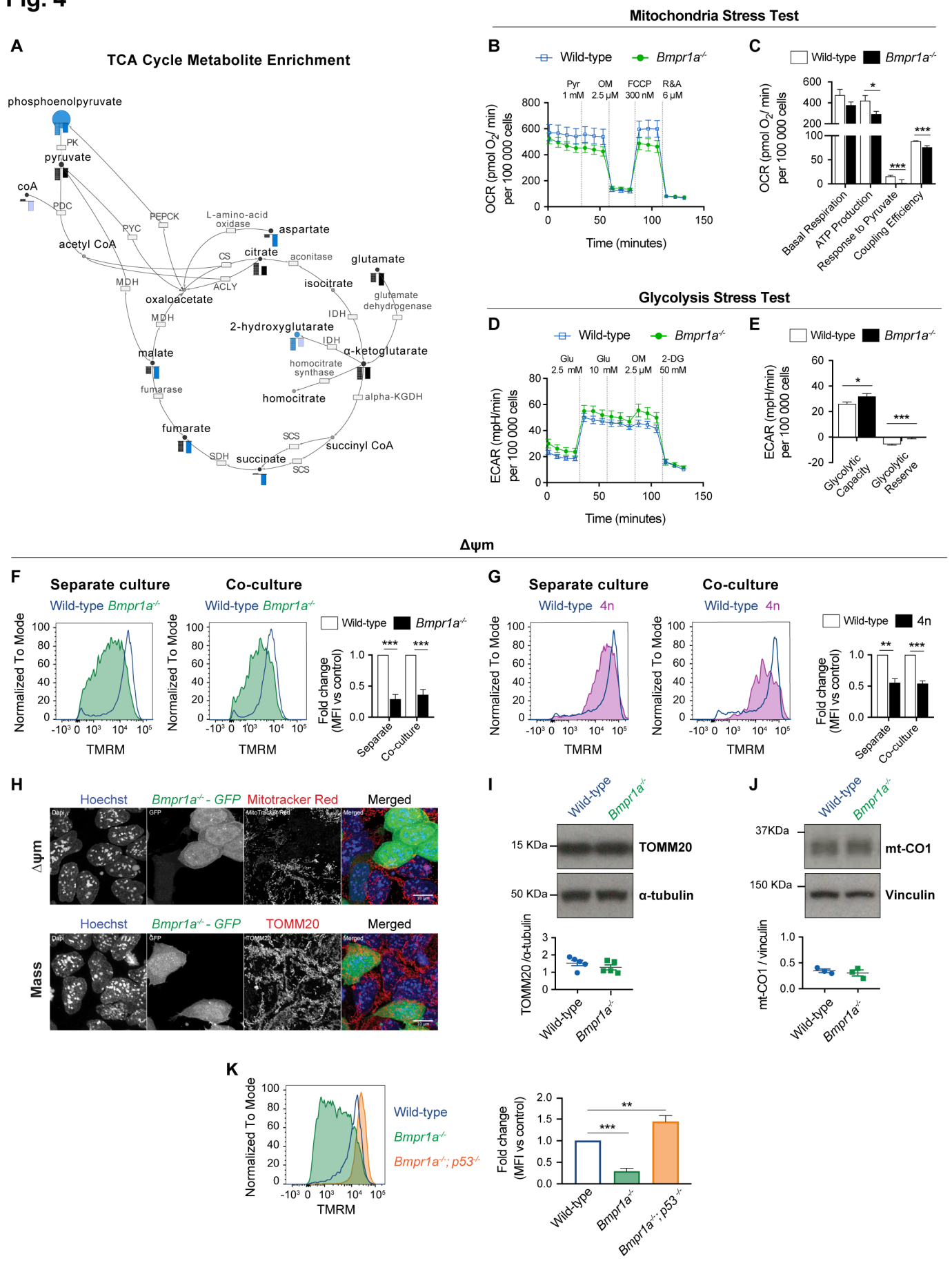
A
TCA Cycle Metabolite Enrichment
phosphoenolpyruvate
PK
pyruvate
coA
PDC
acetyl CoA
PEPCK
PYC
L-amino-acid oxidase
aspartate
citrate
CS
aconitase
glutamate
isocitrate
MDH
ACLY
oxaloacetate
glutamate dehydrogenase
IDH
MDH
2-hydroxyglutarate
IDH
α-ketoglutarate
malate
homocitrate synthase
fumarase
homocitrate
alpha-KGDH
fumarate
SCS
succinyl CoA
SDH
succinate
SCS
Mitochondria Stress Test
B
Wild-type
Bmpr1a-/-
Pyr 1 mM
OM 2.5 µM
FCCP 300 nM
R&A 6 µM
OCR (pmol O2/ min) per 100 000 cells
Time (minutes)
C
Wild-type
Bmpr1a-/-
OCR (pmol O2/ min) per 100 000 cells
Basal Respiration
ATP Production
Response to Pyruvate
Coupling Efficiency
Glycolysis Stress Test
D
Wild-type
Bmpr1a-/-
Glu 2.5 mM
Glu 10 mM
OM 2.5 µM
2-DG 50 mM
ECAR (mpH/min) per 100 000 cells
Time (minutes)
E
Wild-type
Bmpr1a-/-
ECAR (mpH/min) per 100 000 cells
Glycolytic Capacity
Glycolytic Reserve
Δψm
F
Separate culture
Co-culture
Wild-type Bmpr1a-/-
Normalized To Mode
TMRM
Fold change (MFI vs control)
Separate
Co-culture
G
Separate culture
Co-culture
Wild-type 4n
H
Hoechst
Bmpr1a-/- - GFP
Mitotracker Red
Merged
Δψm
Mass
TOMM20
I
Wild-type
Bmpr1a-/-
15 KDa
TOMM20
50 KDa
α-tubulin
TOMM20 /α-tubulin
J
37KDa
mt-CO1
150 KDa
Vinculin
mt-CO1 / vinculin
K
Wild-type
Bmpr1a-/-
Bmpr1a-/-; p53-/-
Normalized To Mode
TMRM
Fold change (MFI vs control)

Fig. 5

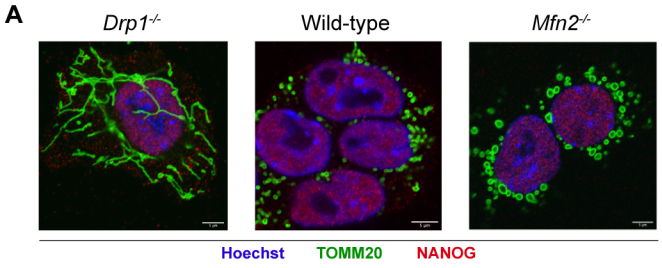
A
Drp1-/-
Wild-type
Mfn2-/-
Hoechst
TOMM20
NANOG

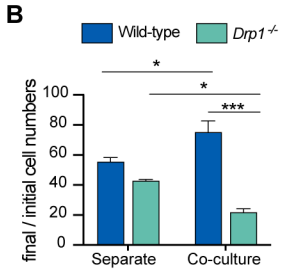
B
Wild-type
Drp1-/-
final / initial cell numbers
100
80
60
40
20
0
*
*
***
Separate
Co-culture

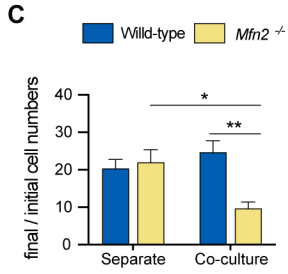
C
Willd-type
Mfn2 -/-
final / initial cell numbers
40
30
20
10
0
*
**
Separate
Co-culture

Fig. 6

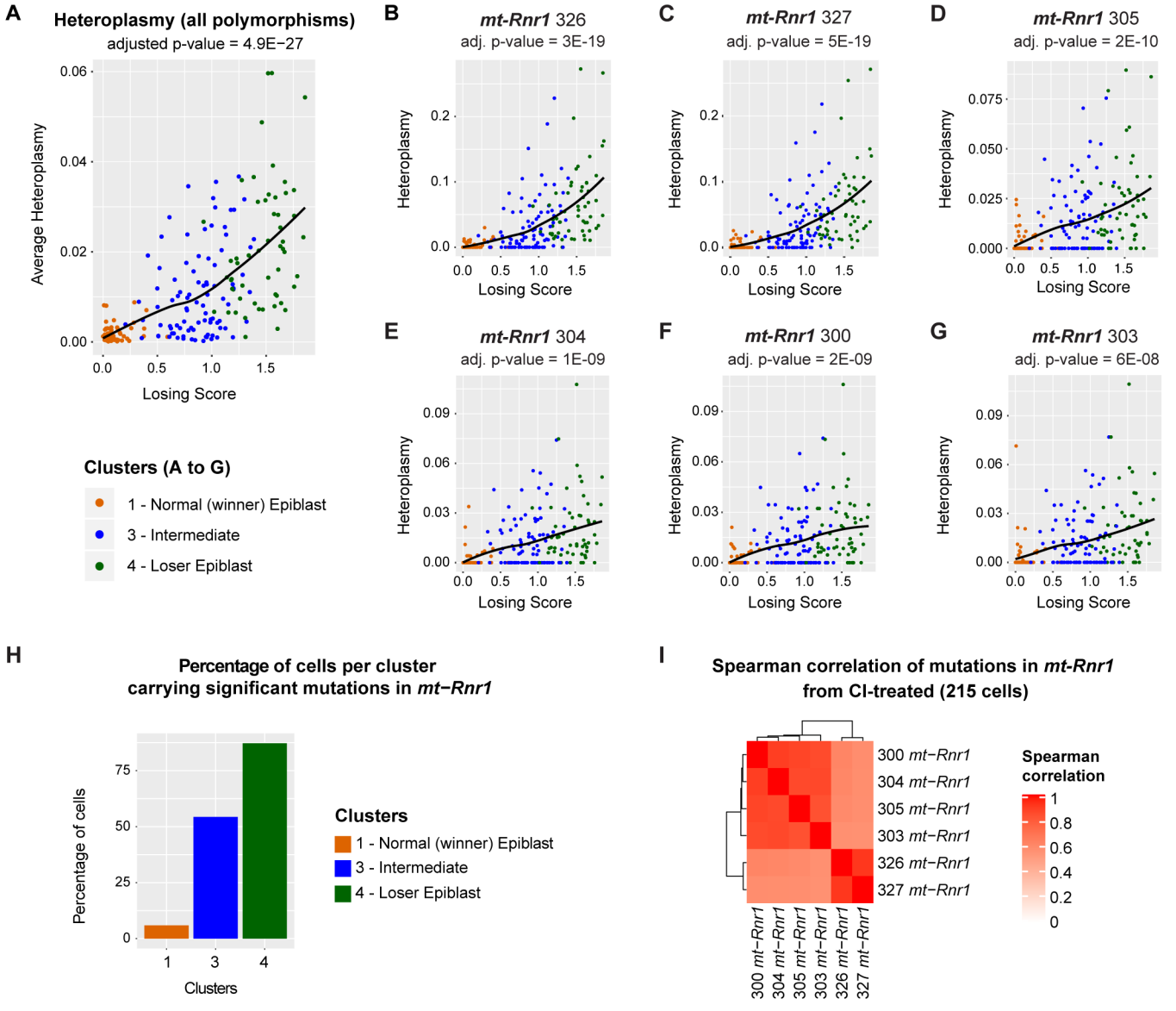
A
Heteroplasmy (all polymorphisms)
adjusted p-value = 4.9E−27
Average Heteroplasmy
Losing Score
B
mt-Rnr1 326
adj. p-value = 3E-19
C
mt-Rnr1 327
adj. p-value = 5E-19
D
mt-Rnr1 305
adj. p-value = 2E-10
E
mt-Rnr1 304
adj. p-value = 1E-09
F
mt-Rnr1 300
adj. p-value = 2E-09
G
mt-Rnr1 303
adj. p-value = 6E-08
Heteroplasmy
Clusters (A to G)
1 - Normal (winner) Epiblast
3 - Intermediate
4 - Loser Epiblast
H
Percentage of cells per cluster carrying significant mutations in mt−Rnr1
Percentage of cells
Clusters
I
Spearman correlation of mutations in mt-Rnr1 from CI-treated (215 cells)
300 mt−Rnr1
304 mt−Rnr1
305 mt−Rnr1
303 mt−Rnr1
326 mt−Rnr1
327 mt−Rnr1
Spearman correlation

Fig. 7

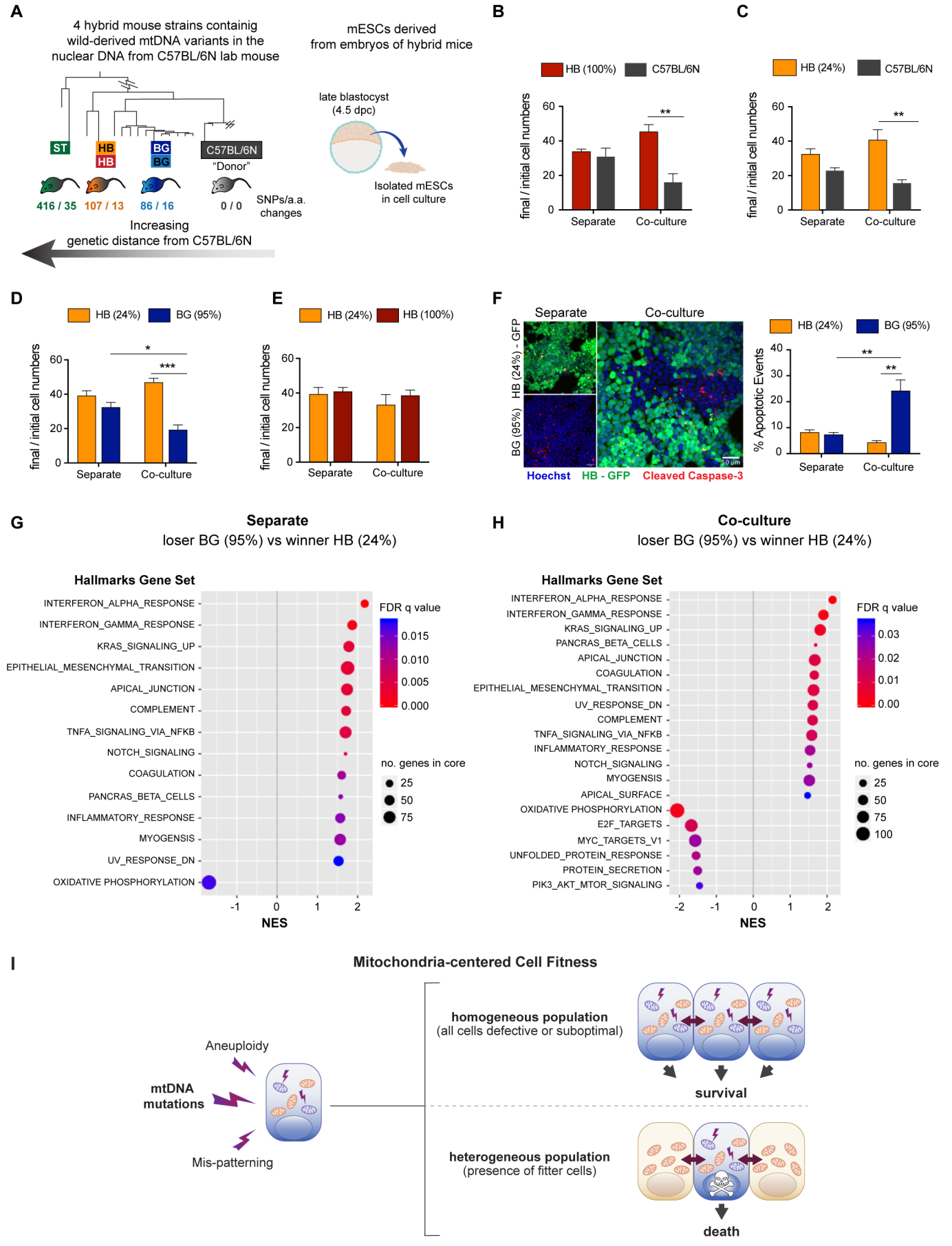
A
4 hybrid mouse strains containig wild-derived mtDNA variants in the nuclear DNA from C57BL/6N lab mouse
mESCs derived from embryos of hybrid mice
ST
HB HB
BG BG
C57BL/6N
"Donor"
416 / 35
107 / 13
86 / 16
0 / 0
SNPs/a.a. changes
late blastocyst (4.5 dpc)
Isolated mESCs in cell culture
Increasing genetic distance from C57BL/6N
B
HB (100%)
C57BL/6N
final / initial cell numbers
Separate
Co-culture
C
HB (24%)
C57BL/6N
D
HB (24%)
BG (95%)
E
HB (24%)
HB (100%)
F
Separate
Co-culture
HB (24%) - GFP
BG (95%)
Hoechst
HB - GFP
Cleaved Caspase-3
% Apoptotic Events
G
Separate
loser BG (95%) vs winner HB (24%)
Hallmarks Gene Set
INTERFERON_ALPHA_RESPONSE
INTERFERON_GAMMA_RESPONSE
KRAS_SIGNALING_UP
EPITHELIAL_MESENCHYMAL_TRANSITION
APICAL_JUNCTION
COMPLEMENT
TNFA_SIGNALING_VIA_NFKB
NOTCH_SIGNALING
COAGULATION
PANCRAS_BETA_CELLS
INFLAMMATORY_RESPONSE
MYOGENSIS
UV_RESPONSE_DN
OXIDATIVE PHOSPHORYLATION
FDR q value
no. genes in core
NES
H
Co-culture
loser BG (95%) vs winner HB (24%)
Hallmarks Gene Set
INTERFERON_ALPHA_RESPONSE
INTERFERON_GAMMA_RESPONSE
KRAS_SIGNALING_UP
PANCRAS_BETA_CELLS
APICAL_JUNCTION
COAGULATION
EPITHELIAL_MESENCHYMAL_TRANSITION
UV_RESPONSE_DN
COMPLEMENT
TNFA_SIGNALING_VIA_NFKB
INFLAMMATORY_RESPONSE
NOTCH_SIGNALING
MYOGENSIS
APICAL_SURFACE
OXIDATIVE PHOSPHORYLATION
E2F_TARGETS
MYC_TARGETS_V1
UNFOLDED_PROTEIN_RESPONSE
PROTEIN_SECRETION
PIK3_AKT_MTOR_SIGNALING
FDR q value
no. genes in core
NES
I
Mitochondria-centered Cell Fitness
Aneuploidy
mtDNA mutations
Mis-patterning
homogeneous population
(all cells defective or suboptimal)
survival
heterogeneous population
(presence of fitter cells)
death

Fig. S1

A

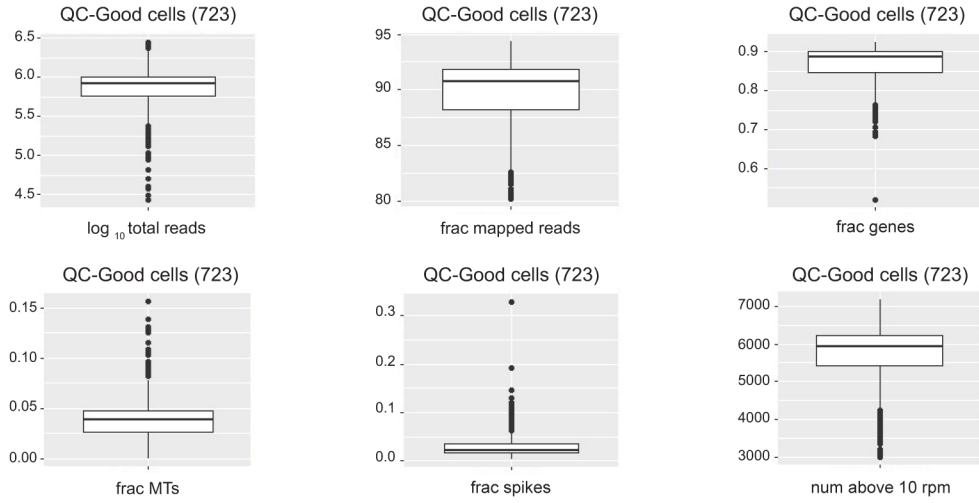

B

Condition\Batch	1	2	3	4	5
CI-treated	136	105	86	16	24
DMSO	132	110	78	15	21

C

Cluster/Batch	1	2	3	4	5
1	147	81	57	7	15
2	45	65	44	7	10
3	46	34	35	13	6
4	23	18	21	2	7
5	7	17	7	2	7

D

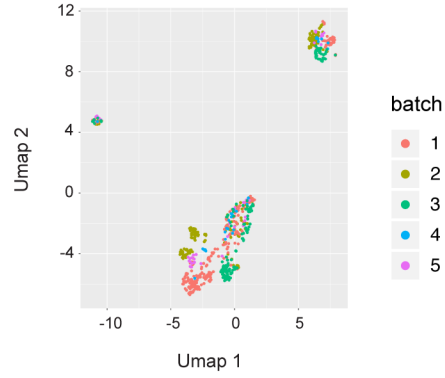

Fig. S2

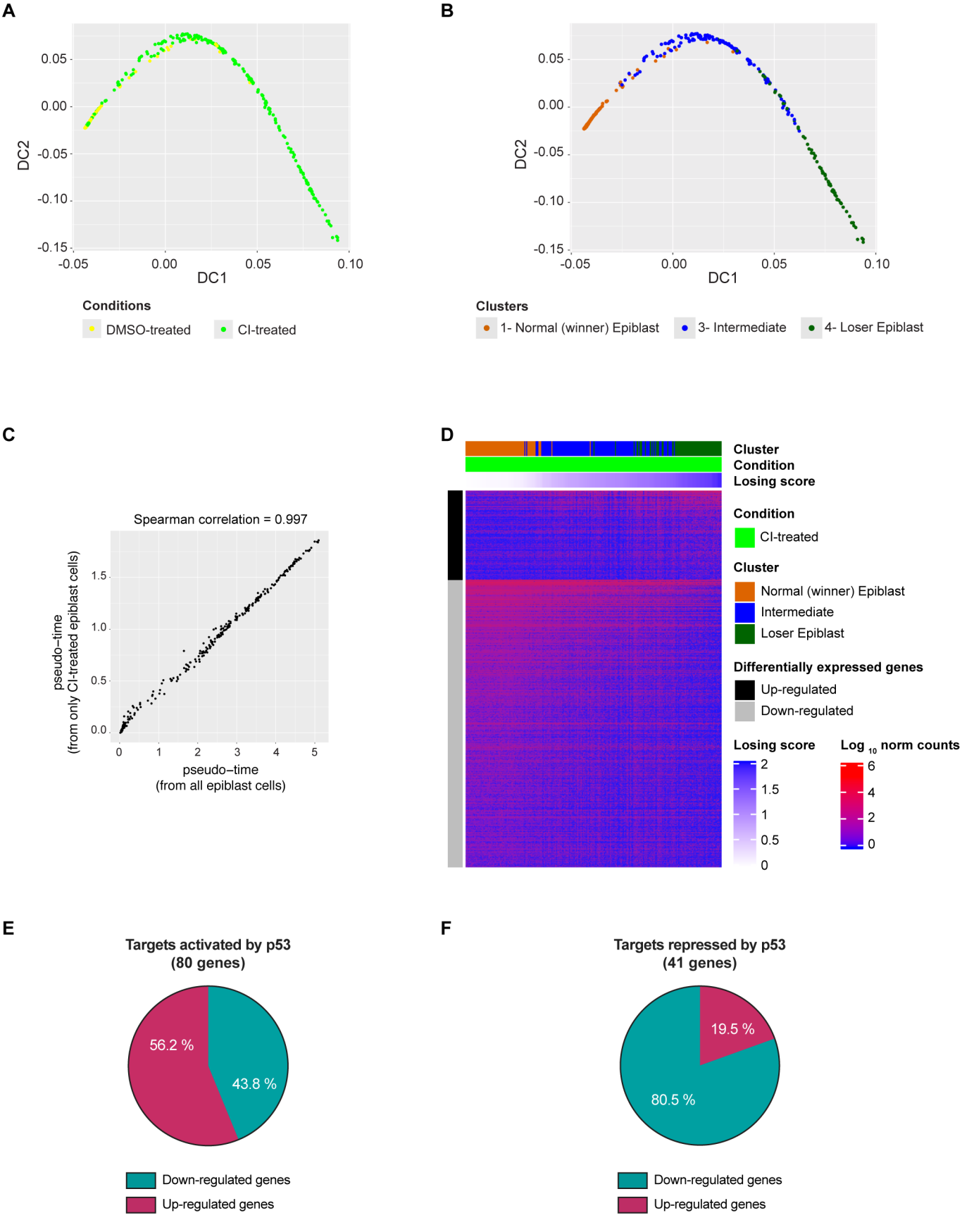
A
DC2
DC1
Conditions
DMSO-treated
CI-treated
B
DC2
DC1
Clusters
1- Normal (winner) Epiblast
3- Intermediate
4- Loser Epiblast
C
Spearman correlation = 0.997
pseudo−time
(from only CI-treated epiblast cells)
pseudo−time
(from all epiblast cells)
D
Cluster
Condition
Losing score
Condition
CI-treated
Cluster
Normal (winner) Epiblast
Intermediate
Loser Epiblast
Differentially expressed genes
Up-regulated
Down-regulated
Losing score
Log 10 norm counts
E
Targets activated by p53
(80 genes)
56.2 %
43.8 %
Down-regulated genes
Up-regulated genes
F
Targets repressed by p53
(41 genes)
19.5 %
80.5 %
Down-regulated genes
Up-regulated genes

Fig. S3

A

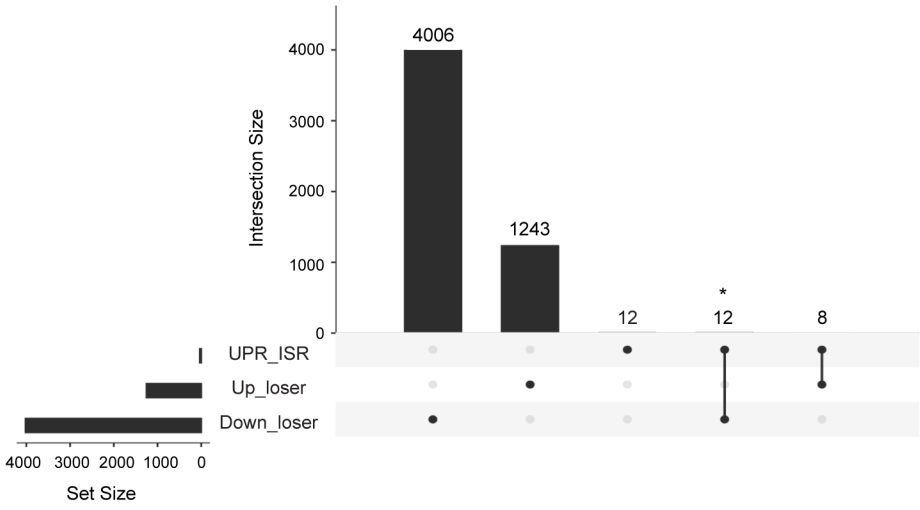

B

Gene	FDR	Rank
Ddit3	4.63E-39	2
Atf3	6.08E-27	22
Atf4	2.14E-23	31
Foxo3	2.69E-22	37
Ppp1r15a	8.33E-18	68
Eif2ak3	7.17E-13	150
Nfe2l2	1.55E-10	207
Gdf15	5.53E-08	333

C

Gene	FDR	Rank
Mthfd1l	2.54E-35	147
Hspe1	8.71E-34	164
Cat	2.44E-30	219
Hspd1	6.93E-13	1262
Sod2	1.25E-10	1551
Hsph1	4.48E-10	1655
Lonp1	1.08E-06	2348
Eif2a	1.49E-06	2382
Mthfd2	1.31E-05	2693
Hspa4	2.84E-05	2790
Cth	2.53E-03	3677
Nrf1	2.86E-03	3698

D

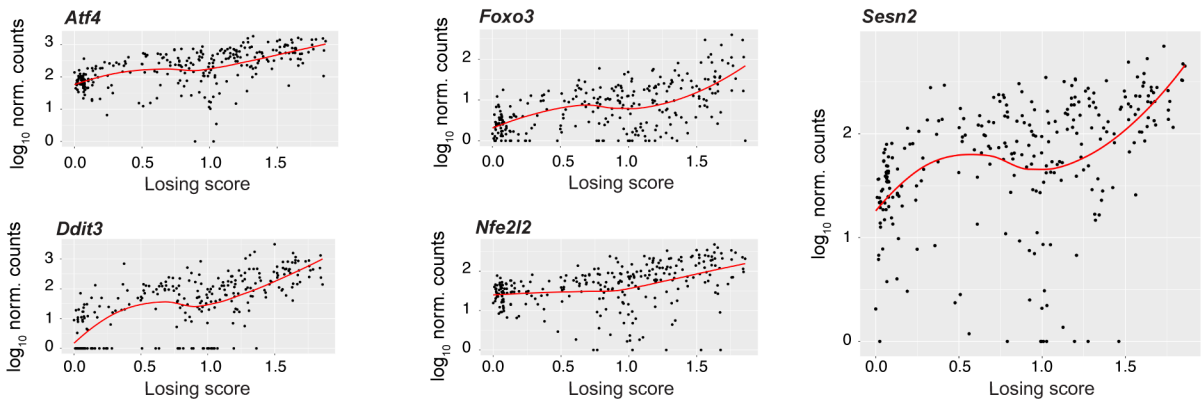

E

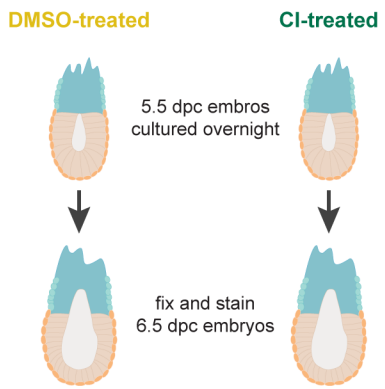

F

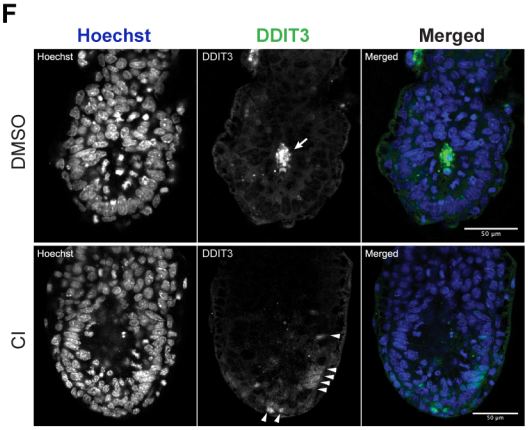

G

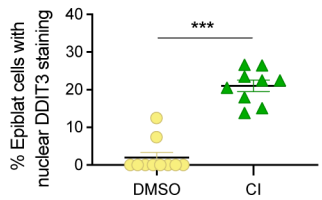

Fig. S4

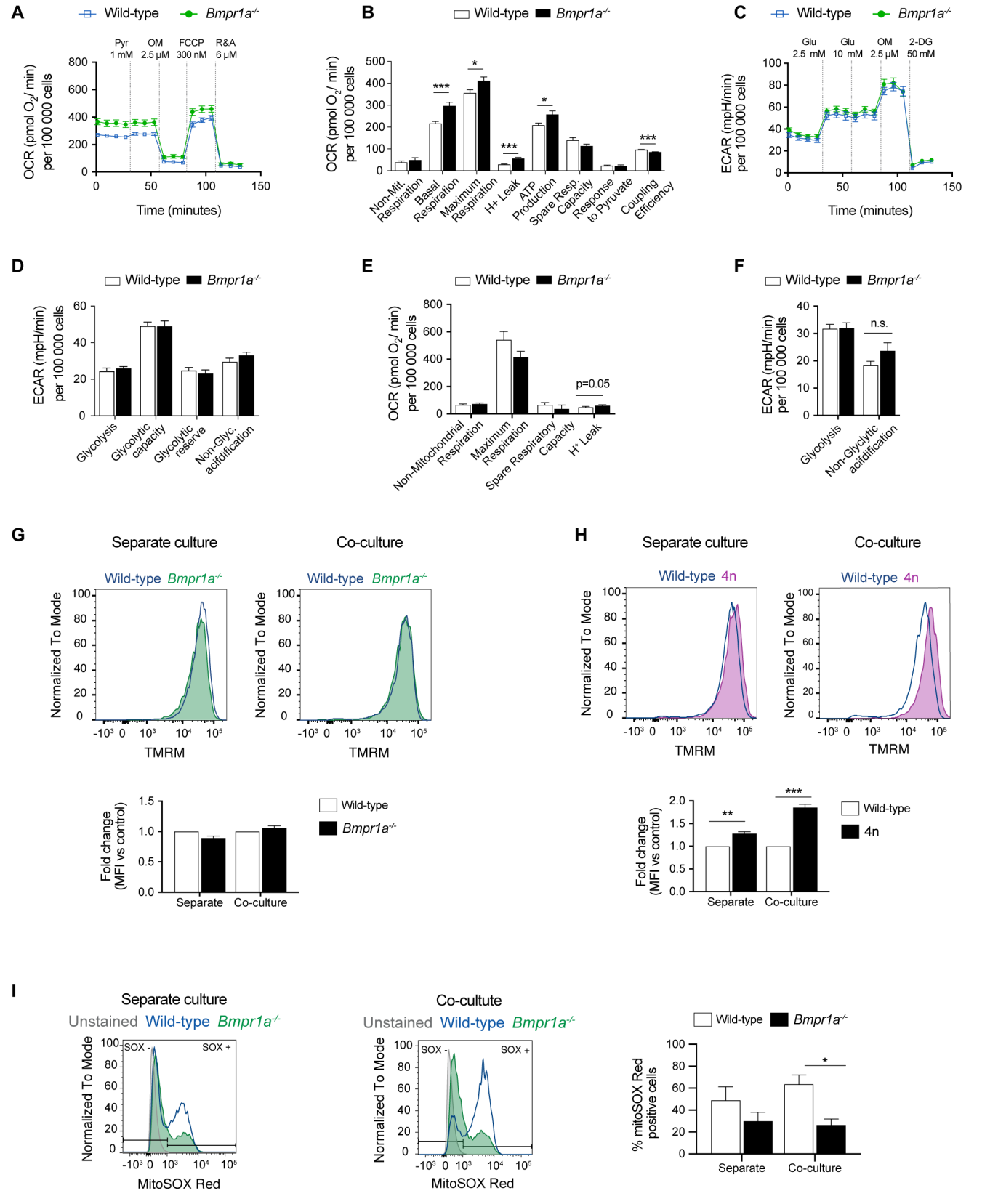
A
Wild-type
Bmpr1a-/-
Pyr 1 mM
OM 2.5 µM
FCCP 300 nM
R&A 6 µM
OCR (pmol O2/ min) per 100 000 cells
Time (minutes)
B
Wild-type
Bmpr1a-/-
OCR (pmol O2/ min) per 100 000 cells
Non-Mit. Respiration
Basal Respiration
Maximum Respiration
H+ Leak
ATP Production
Spare Resp. Capacity
Response to Pyruvate
Coupling Efficiency
C
Wild-type
Bmpr1a-/-
Glu 2.5 mM
Glu 10 mM
OM 2.5 µM
2-DG 50 mM
ECAR (mpH/min) per 100 000 cells
Time (minutes)
D
Wild-type
Bmpr1a-/-
ECAR (mpH/min) per 100 000 cells
Glycolysis
Glycolytic capacity
Glycolytic reserve
Non-Glyc. acidification
E
Wild-type
Bmpr1a-/-
OCR (pmol O2/ min) per 100 000 cells
p=0.05
Non-Mitochondrial Respiration
Maximum Respiration
Spare Respiratory Capacity
H+ Leak
F
Wild-type
Bmpr1a-/-
ECAR (mpH/min) per 100 000 cells
n.s.
Glycolysis
Non-Glycolytic acidification
G
Separate culture
Co-culture
Wild-type Bmpr1a-/-
Normalized To Mode
TMRM
Fold change (MFI vs control)
Separate
Co-culture
Wild-type
Bmpr1a-/-
H
Separate culture
Co-culture
Wild-type 4n
Normalized To Mode
TMRM
Fold change (MFI vs control)
Separate
Co-culture
Wild-type
4n
I
Separate culture
Unstained Wild-type Bmpr1a-/-
SOX -
SOX +
Normalized To Mode
MitoSOX Red
Co-cultute
Unstained Wild-type Bmpr1a-/-
SOX -
SOX +
Normalized To Mode
MitoSOX Red
Wild-type
Bmpr1a-/-
% mitoSOX Red positive cells
Separate
Co-culture

Fig. S5

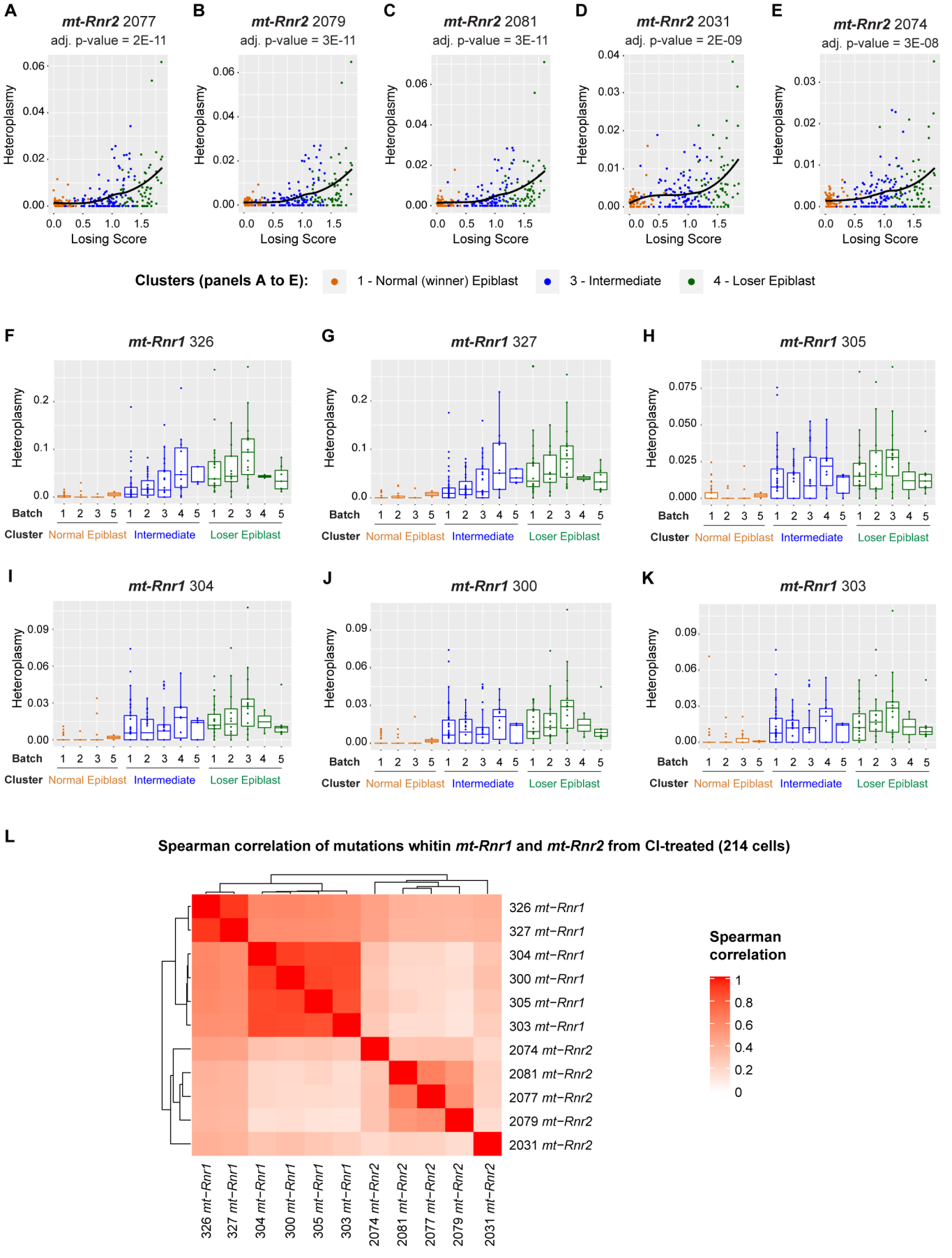
A
mt-Rnr2 2077
adj. p-value = 2E-11
B
mt-Rnr2 2079
adj. p-value = 3E-11
C
mt-Rnr2 2081
adj. p-value = 3E-11
D
mt-Rnr2 2031
adj. p-value = 2E-09
E
mt-Rnr2 2074
adj. p-value = 3E-08
Heteroplasmy
Losing Score
Clusters (panels A to E):
1 - Normal (winner) Epiblast
3 - Intermediate
4 - Loser Epiblast
F
mt-Rnr1 326
G
mt-Rnr1 327
H
mt-Rnr1 305
I
mt-Rnr1 304
J
mt-Rnr1 300
K
mt-Rnr1 303
Batch
Cluster
Normal Epiblast
Intermediate
Loser Epiblast
L
Spearman correlation of mutations whitin mt-Rnr1 and mt-Rnr2 from CI-treated (214 cells)
326 mt−Rnr1
327 mt−Rnr1
304 mt−Rnr1
300 mt−Rnr1
305 mt−Rnr1
303 mt−Rnr1
2074 mt−Rnr2
2081 mt−Rnr2
2077 mt−Rnr2
2079 mt−Rnr2
2031 mt−Rnr2
Spearman correlation

Fig. S6

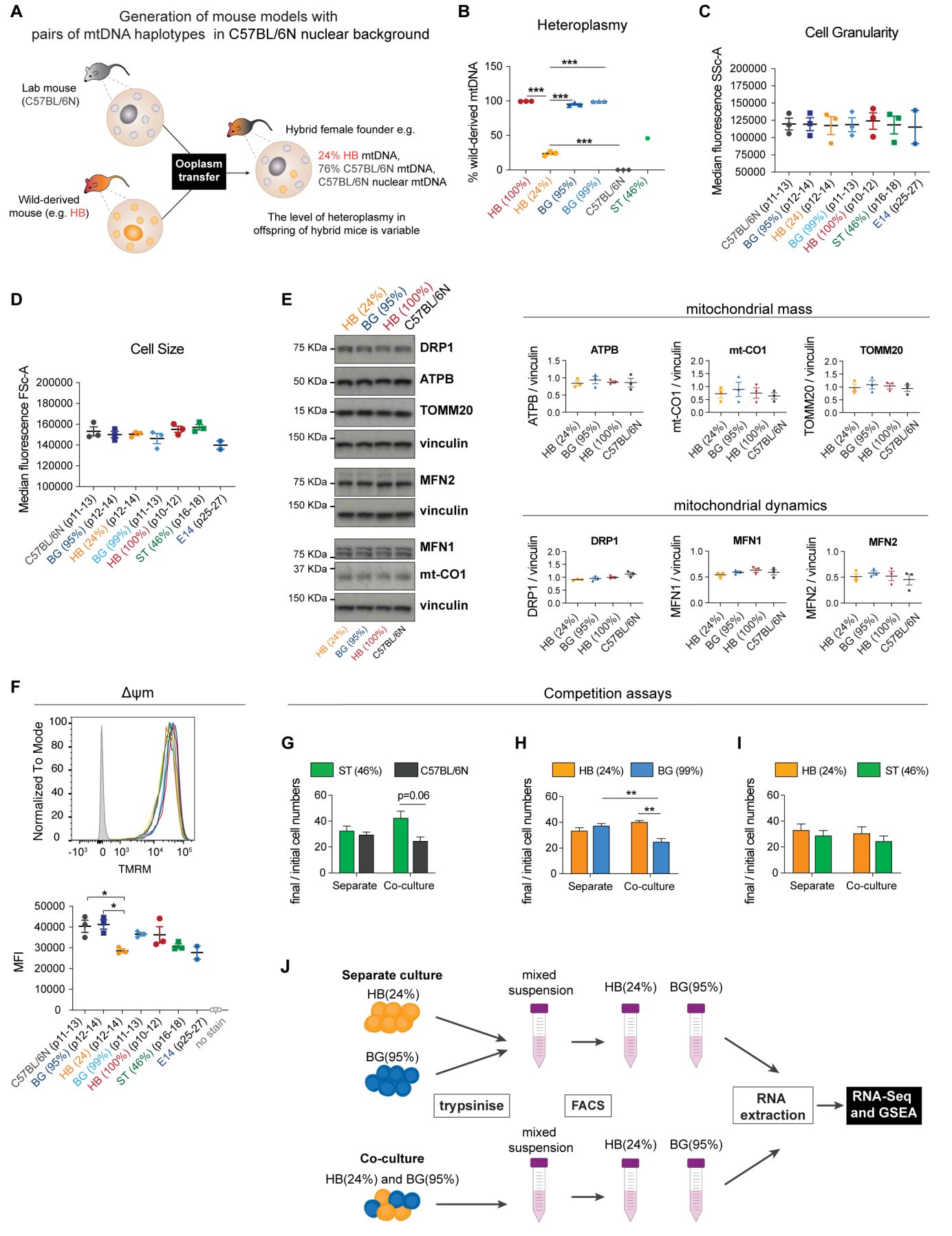
A
Generation of mouse models with pairs of mtDNA haplotypes in C57BL/6N nuclear background
Lab mouse (C57BL/6N)
Wild-derived mouse (e.g. HB)
Ooplasm transfer
Hybrid female founder e.g.
24% HB mtDNA, 76% C57BL/6N mtDNA, C57BL/6N nuclear mtDNA
The level of heteroplasmy in offspring of hybrid mice is variable
B
Heteroplasmy
% wild-derived mtDNA
HB (100%)
HB (24%)
BG (95%)
BG (99%)
C57BL/6N
ST (46%)
C
Cell Granularity
Median fluorescence SSc-A
D
Cell Size
Median fluorescence FSc-A
E
HB (24%)
BG (95%)
HB (100%)
C57BL/6N
DRP1
ATPB
TOMM20
vinculin
MFN2
MFN1
mt-CO1
mitochondrial mass
mitochondrial dynamics
F
Δψm
Normalized To Mode
TMRM
MFI
no stain
Competition assays
G
ST (46%)
C57BL/6N
p=0.06
final / initial cell numbers
Separate
Co-culture
H
HB (24%)
BG (99%)
I
J
Separate culture
mixed suspension
trypsinise
FACS
RNA extraction
RNA-Seq and GSEA
Co-culture
HB(24%) and BG(95%)

Fig. S7

A

Source	Term	Adjusted p-value
GO:CC	mitochondrial protein complex	5.91E-05
GO:CC	inner mitochondrial membrane protein complex	8.84E-04
GO:CC	mitochondrial inner membrane	8.93E-04
GO:CC	mitochondrial respirasome	2.44E-03
GO:CC	respiratory chain complex	3.89E-03
GO:CC	respirasome	6.50E-03
GO:CC	mitochondrial part	1.06E-02
GO:CC	organelle inner membrane	4.65E-02
KEGG	oxidative phosphorylation	7.71E-04
KEGG	Huntington disease	2.35E-03
WP	electron transport chain	1.26E-03

B

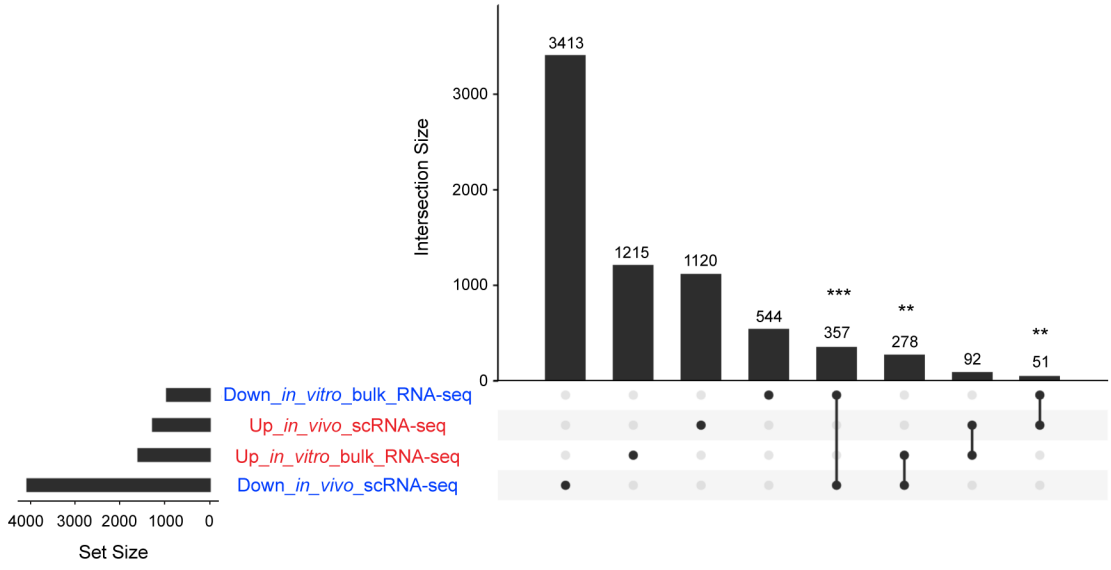
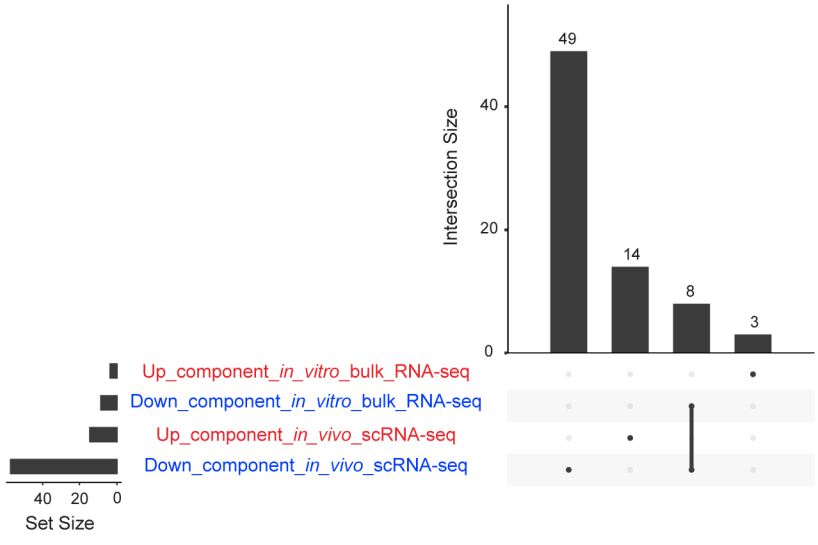
C